Size stability of nanostructures in Stranski-Krastanow systems under an electric field

Zhijun Huang and Cheng-hsin Chiu*
Department of Materials Science and Engineering, National University of Singapore, Singapore 117576, Singapore
(Received 24 March 2008; revised manuscript received 21 July 2008; published 8 September 2008)

This paper investigates the stability of wires against size variation for Stranski-Krastanow systems under the influence of an electric field generated by a patterned electric plate. The stability is determined by considering the total energy change as a function of the wire size. The results show that the wire size can be stabilized by the electric field if the system meets the viability criterion and the effective electric field effect is within the minimum and maximum limits. The minimum limit ensures that the wire formation is energetically favorable at moderate sizes, while the maximum limit enforces the suppression of the formation of large wires.

DOI: 10.1103/PhysRevB.78.125405 PACS number(s): 68.55.−a, 81.16.Dn

I. INTRODUCTION

The self-assembly of nanoislands on the Stranski-Krastanow (SK) systems is an attractive method for fabricating nanodevices. In this method, a flat film is grown heteroepitaxially on a thick substrate. The flat film then develops into nanostructures on a flat wetting layer when exceeding the critical thickness for the SK transition.[1,2] The method is appealing for its capability to manufacture nanostructures by self-organization with high material quality and unique electronic, magnetic, and optical properties.[1–3] The method, however, encounters the problem that the self-organized nanoislands are unstable against coarsening, resulting in a wide distribution of island size.[4,5] Besides the problem of island coarsening, the method also faces difficulties in controlling the shapes and sites of the nanoislands.

Many schemes have been suggested in the literature to overcome the challenges in the self-assembly of nanoislands on the SK systems. The schemes can be generally classified into three categories. The first one is to enhance the material properties of the SK systems such as the surface stress[6–8] and the film-substrate interaction[9,10] in order to induce island arrays that are stable against coarsening.

In comparison, the second category employs embedded structures to improve the uniformity of the island size and spacing. The embedded structures can be multiple arrays of nanoislands separated by layers of a different material.[11–21] The embedded structures can also be the misfit dislocations in the strained film[22–24] or a regular dislocation network generated by bonding a film onto a substrate of the same material but with a twist and/or miscut between them.[25–27]

The third category exploits special features on the film surface to control the growth of nanoislands. The features can be fabricated by lithography, which include mesas,[28–35] pit arrays,[36–40] patterned oxide masks,[41–43] micropatterning by focused ion beams,[44] thin patterned films,[45] microdisks,[46] and gold patterns.[47] The surface features can also be generated by novel techniques adopted in the growth process. Examples include activating step bunching to produce regular ripples on vicinal surfaces,[48] embedding hard particles in a buffer layer to yield valleys on the surface,[49–52] and fast deposition of heteroepitaxial films to cause shallow holes on the film surface.[53–55]

The schemes in the three categories provide inspiring ideas for controlling the self-assembly of nanoislands. Those schemes, however, either adopt complex manufacture steps, e.g., lithography, prior to the self-assembly process, or lack full control over the size, shape, and site of each nanostructure. Realizing controllable self-assembly via a simple process is still a challenging issue in the nanotechnology.

A proposed alternative is to apply an electric field. This approach was first adopted in the lithographically induced self-assembly (LISA) where a liquid polymeric film on a thick substrate was exposed to an electrode with the gap between the film and the electrode being filled with air[56,57] and/or another liquid layer.[58–60] The system was then subject to an electric field to induce viscous flow on the liquid film in order to form structures.[61,62] The scheme has the capability to use patterns on the electrode to manipulate the size, shapes, and sites of the structures, while the scheme has the disadvantage of dielectric breakdown, long-range disordering, and structure coalescence.[63–65]

More recently, it was suggested that electric fields generated by patterned electrodes could also be an effective prescription for resolving the issues in the self-assembly of nanoislands in the SK systems; the idea was termed the electromolding self-organization (EMSO) process.[66] Numerical simulation for the EMSO process indicates the process is capable of fabricating a wide range of island shapes, including 2×2 island arrays, square rings, cross junctions, and zigzag ridges, with controllable sizes and locations. The EMSO process also has the crucial advantage that the process can produce nanostructures stable against size variation.[66] The unique feature is in contrast to the common problem of unstable islands in the SK systems and in the LISA method.

The previous study clearly pointed out the potential of the EMSO process to produce nanoislands on the SK systems stable against size variation.[66] The analysis of that study, however, focused on specific examples. The size stability of faceted nanostructures on general SK systems during the EMSO process has not been fully understood.

The size stability is examined in this paper by analyzing the total energy changes due to the formation of faceted nanostructures. Our investigation focuses on the two-dimensional (2D) cases, and of particular interest is the scenario where the height of the electric plate is much larger than the wire size. The results reveal that the size stability can be achieved in the EMSO process if the material properties and the film thickness of the SK system satisfy the

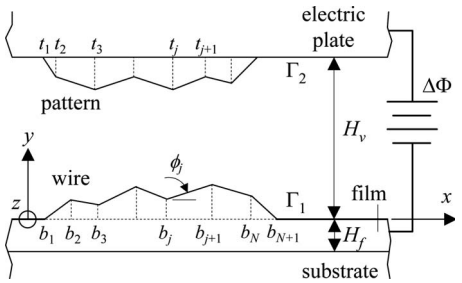

FIG. 1. Schematic diagram of a heteroepitaxial film-substrate system containing a faceted nanostructure on a flat wetting layer of thickness H_f; the system is exposed to a patterned electric plate at a height of H_v.

viability criterion expressed in Eq. (48), and the effective electric field effect is within the upper and lower limits. The results illuminate a clear overall picture for understanding how the size stability is affected by the vast amount of parameters involved in the EMSO process, including the material properties of the SK system, the film thickness, the electric plate height, and the size and slope of the pattern on the electric plate.

The paper is organized as follows: The paper first summarizes the methods for calculating the total energy change due to the formation of a faceted wire in Sec. II, and then describes the model problem adopted for the stability analysis in Sec. III. After presenting the methods and the model problem, the paper shows the results in four sections: Section IV examines the size stability of the SK systems without the electric field. Section V adopts a coarsening SK system to investigate the effects of the electric field on the size stability. Section VI derives the stability condition for the case where the electric plate height is large. Section VII studies how the size stability is affected by misalignment between the wire and the pattern on the electric plate. The paper concludes with a discussion in Sec. VIII and a summary of the results in Sec. IX.

II. ENERGY OF NANOSTRUCTURES IN THE SK SYSTEMS

This section discusses the first-order boundary perturbation method for evaluating the total energy change due to the formation of a nanoisland on the SK film-substrate system. The total mass of the film is conserved during the island formation, and the whole system is subject to an electric field generated by a patterned electrode. For simplicity, the discussion is limited to 2D cases.

A. SK film-substrate structure under an electric field

Figure 1 plots a SK system consisting of a thick substrate, a thin conductor film, and an electric plate at a height of H_v above the film. The electric plate and the film are connected by a battery with the voltage being fixed at $\Delta\Phi$.

The system is attached by a set of Cartesian coordinate axes on the film surface Γ_1. The x and z axes are parallel to the surface, while the y axis is normal to the surface.

The conductor film of the system contains a flat wetting layer of thickness H_f and a nanowire with N facets. There are totally $N+1$ vertices on the structures; the x components on the vertices are denoted as $\mathcal{B}=\{b_1,b_2,\ldots,b_{N+1}\}$. The angle between the jth facet and the x direction is ϕ_j. For convenience, one of the angles, denoted as ϕ^*, is chosen to define the characteristic slope $\mathcal{S}=\tan\phi^*$ of the structure. The ratio between the slope of the jth facet and the characteristic value $\mathcal{S}$ gives the relative slope m_j of the facet, i.e., $m_j=\tan\phi_j/\mathcal{S}$.

In addition to the nanostructure on the film surface Γ_1, the system also exhibits a pattern of $\mathcal{N}$ facets on the electric plate surface Γ_2. The geometry of the pattern can be fully described by the characteristic slope $\mathcal{S}_e$ of the pattern, the relative slopes of the $\mathcal{N}$ facets $\{l_1,l_2,\ldots,l_{\mathcal{N}+1}\}$, and the x components of the vertices on the pattern $\mathcal{T}=\{t_1,t_2,\ldots,t_{\mathcal{N}+1}\}$.

The film and the substrate are elastically similar materials characterized by the shear modulus μ and Poisson's ratio ν. The film and the substrate are subject to a mismatch strain $\mathcal{E}_0$ between them, which results in deformation and strain energy in the system. In addition to the strain energy, the SK system considered here is also affected by the electrostatic energy, the film-substrate interaction energy, and the surface energy. The changes of the four types of energy during the wire formation are the key quantities in our analyses; the solution procedure of calculating the energy changes under the condition of mass conservation is presented in the subsequent subsections.

B. Strain energy change

The strain energy change ΔW_σ due to the formation of the nanostructure can be estimated by the first-order boundary perturbation method for solving the elasticity problems of a strained film on a thick substrate.[67–70] The starting point of the method is to determine the strain energy density $w_\sigma(x)$ on the islanded film surface accurate to the first order of $\mathcal{S}$,[67]

$$w_\sigma(x) = w_{\sigma 0}^{3d} - 2w_{\sigma 0}\mathcal{S}\Psi_\sigma(x), \tag{1}$$

where $w_{\sigma 0}=\mu(1+\nu)^2\mathcal{E}_0^2/(1-\nu)$, $w_{\sigma 0}^{3d}=2w_{\sigma 0}/(1+\nu)$, and the function $\Psi_\sigma(x)$ illustrates the variation of $w_\sigma(x)$ on the film due to the nanowire,

$$\Psi_\sigma(x) = -\frac{2}{\pi}\sum_{j=1}^{N} m_j \Re\left[\ln\frac{x-b_{j+1}}{x-b_j}\right]. \tag{2}$$

The symbol $\Re$ in Eq. (2) denotes the real part of a complex number.

The result of $w_\sigma(x)$ is then used to evaluate the variation of the strain energy δW_σ with that of the surface profile $\delta f(x)$ according to the following formula:[67,68,71,72]

$$\delta W_\sigma = \int w(x)\,\delta f(x)\,dx. \tag{3}$$

Carrying out the integration in Eq. (3) and requiring that the total film volume remains the same as $f(x)$ changes from a flat surface to an islanded profile yields the strain energy change ΔW_σ,[67]

$$\Delta W_\sigma = - w_{\sigma 0} \mathcal{S} V U_\sigma, \tag{4}$$

where V is the volume of the nanowire, and U_σ refers to the effect of the nanostructure shape on ΔW_σ,

$$U_\sigma = \frac{1}{V} \int_{\mathcal{B}} \Psi_\sigma(x) f(x) dx. \tag{5}$$

The quantity U_σ is a constant for self-similar wires with different size.

C. Interaction energy change

1. Formulas

The film-substrate interaction accounts for the SK transition and the development of the wetting layer.[9,73,74] The interaction can be modeled as a special type of film surface energy of which the density g varies with the distance $y + H_f$ between the film surface and the film-substrate interface.[9] When the interaction is caused by the quantum confinement, the density is expressed as $g(y) = B/(y+H_f)$, where B is a material property.[74] It is assumed that the interaction is not affected by the electric field.

The change of the interaction energy is determined by

$$\Delta E_I = \int g d\Gamma_{\mathcal{B}} + \int g d\Gamma_w - \int g d\Gamma_0, \tag{6}$$

where $d\Gamma_{\mathcal{B}}$ refers to the area integral over the wire facets, $d\Gamma_w$ represents that over the wetting layer surface, and $d\Gamma_0$ denotes that over the flat film surface before the wire formation.

The area integral $d\Gamma_{\mathcal{B}}$ can be expressed as $d\Gamma_{\mathcal{B}} = (\mathcal{S}m)^{-1} dx$; substituting the expression into the first term in Eq. (6) yields

$$\int g d\Gamma_{\mathcal{B}} = \sum_{j=1}^{N} \frac{1}{\sin \phi_j} [\mathcal{G}(y_{j+1}) - \mathcal{G}(y_j)], \tag{7}$$

where y_j is the y component of the jth vertices of the wire and $\mathcal{G}(y)$ is defined by

$$\mathcal{G}(y) = \int g(y) dy. \tag{8}$$

The function $\mathcal{G}(y)$ is simplified to $\mathcal{G}(y) = B \ln(y + H_f)$ if the quantum confinement is the mechanism of the film-substrate interaction.

Turn to the second and the third terms in Eq. (6). The third term refers to the interaction energy of the system prior to the wire formation, and is given by $g(H_f)A$, where A is the area of the flat film surface. The second term, on the other hand, corresponds to the interaction energy of the flat wetting layer after the wire formation, and can be expressed as $g(H_f - \Delta H_f)(A - b)$, where $b = b_{N+1} - b_1$ is the width of the wire base, $H_f - \Delta H_f$ is the thickness of the wetting layer after the wire formation, and $\Delta H_f = V/A$. By evoking the conditions $A \gg b$ and $H_f \gg \Delta H_f$, the difference between the second and the third terms can be calculated to be

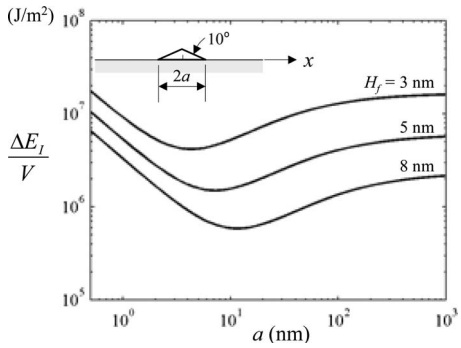

FIG. 2. The variation of $\Delta E_I/V$ with the base width of a triangular wire at different film thickness (H_f=3, 5, and 8 nm). The facet angle ϕ of the wire is 10° and the interaction energy strength B of the film is 1.5×10^{-10} J/m^2.

$$g(H_f - \Delta H_f)(A - b) - g(H_f)A = - g'(H_f)V - g(H_f)b. \tag{9}$$

Adding Eqs. (7) and (9) determines the change of the interaction energy,

$$\Delta E_I = \sum_{j=1}^{N} \frac{\mathcal{G}(y_{j+1}) - \mathcal{G}(y_j)}{\sin \phi_j} - g(H_f)(b_{N+1} - b_1) - g'(H_f)V. \tag{10}$$

The result is further discussed in Sec. II C 2 with the focus on the case where the interaction is dominated by the quantum confinement mechanism.

2. Effects of interaction energy on wire formation

The interaction energy change ΔE_I expressed in Eq. (10) consists of three terms. The first two evaluate the difference between the interaction energy on the wire surface and that on the film surface with the area equal to that of the wire base. In a sense, the difference is similar to the surface energy change during the wire growth except that the interaction energy density decreases with the height of the wire. Because of the similarly, the first two terms are called the area contribution of ΔE_I. The area contribution is positive at small wire sizes and decreases to be negative as the wire size increases.

The third term in Eq. (10), on the other hand, refers to the interaction energy change caused by the decrease in the wetting layer thickness during the formation of wire under the condition of mass conservation. Since this part of change is proportional to the wire volume V, this part is called the volume contribution of ΔE_I; the volume contribution is positive.

After identifying the area and volume contributions of the interaction energy, we examine the variation of $\Delta E_I/V$ with the size of a triangular wire at different film thickness. The facet angle ϕ of the wire is 10°, and the interaction energy strength B is taken to be 1.5×10^{-10} J/m. The results, depicted in Fig. 2, show three characteristics of $\Delta E_I/V$. First, $\Delta E_I/V$ is positive, suggesting the interaction energy suppresses the formation of wires. Second, $\Delta E_I/V$ is a constant when the wire size is sufficiently large. The constant corresponds to the volume contribution of the interaction energy

and is larger on thinner films. Third, and most importantly, $\Delta E_I/V$ exhibits a minimum. Similar to the second characteristic, the depth of the minimum is also larger on thinner films.

The volume contribution and the minimum of $\Delta E_I/V$ illuminate how the wires in the SK systems can be stabilized against size variation. The size stability is achieved when the system meets the conditions that the formation of wires is energetically unfavorable for large wires but favorable for moderate ones. To satisfy the first condition, the strength of the volume contribution of ΔE_I has to be sufficiently large in order to compete with the reduction of the strain and electrostatic energy, which is also proportional to the wire volume. (The change of the electrostatic energy is discussed later in Sec. II D.) Since the volume contribution of the interaction energy increases with decreasing thickness, the first condition can be fulfilled when the thickness is below a critical value.

The first condition ensures that the growth of large wires is suppressed; however, wires of moderate sizes may still form because of the minimum in $\Delta E_I/V$. The formation of moderate wires is controlled by the interaction energy strength B and the thickness of the film. A strong interaction increases the depth of the minimum of $\Delta E_I/V$, thus favoring the wire formation. The film thickness, on the other hand, needs to be higher than a minimum value for wire formation and lower than the critical value for the first condition.[75] In addition to the interaction energy strength and the film thickness, the size stability is also affected by the pattern on the upper electric plate. Discussion of this issue is delayed until we present the formulas for calculating the electrostatic energy change due to wire formation in Sec. II D.

In short, the size stability is realized when the volume contribution of the interaction energy can suppress the development of large wires, and at the same time, the minimum in $\Delta E_I/V$ allows the growth of moderate wires. More quantitative analyses of the size stability are presented later in Sec. IV for SK systems without an electric field and in Secs. V–VII for SK systems influenced by patterned electric plates.

D. Electrostatic energy change

1. Formulas

This section examines the electrostatic energy change ΔW_e due to the nanostructure formation on the film surface where the formation is affected by the preexisting pattern of the electric plate and is under the condition of film volume conservation. The solution procedure for evaluating ΔW_e is similar to that for ΔW_σ. The first step is to derive the electrostatic energy density $w_e(x)$ on the film surface by the first-order perturbation method,

$$w_e = w_{e0} + 2w_{e0}\mathcal{S}\Psi_1(x) + 2w_{e0}\mathcal{S}_e\Psi_2(x), \tag{11}$$

where $w_{e0}=\epsilon_0\Delta\Phi^2/(2H_v^2)$, ϵ_0 is the permittivity of vacuum, $\Psi_1(x)$ expresses the variation of $w_e(x)$ due to the nanowire, and $\Psi_2(x)$ corresponds to that due to the pattern on the upper electric plate. The two functions, $\Psi_1(x)$ and $\Psi_2(x)$, are found to be

$$\Psi_1(x) = -\frac{1}{\pi}\Re\left\{\sum_{j=1}^{N} m_j \ln\left[\frac{e^{\eta(x-b_{j+1})}-1}{e^{\eta(x-b_j)}-1}\right]\right\}, \tag{12}$$

$$\Psi_2(x) = \frac{1}{\pi}\Re\left\{\sum_{j=1}^{\mathcal{N}} l_j \ln\left[\frac{e^{\eta(x-t_{j+1})}+1}{e^{\eta(x-t_j)}+1}\right]\right\}, \tag{13}$$

where $\eta=\pi/H_v$.

After obtaining $w_e(x)$, the second step considers the variation of the electrostatic energy δW_e with that of the surface profile δf,

$$\delta W_e = -\int w_e(x)\,\delta f(x)dx. \tag{14}$$

Substituting Eq. (11) into Eq. (14) and taking into account the conservation of the film volume during the film morphology variation yields

$$\Delta W_e = -w_{e0}\mathcal{S}VU_1 - 2w_{e0}\mathcal{S}_eVU_2, \tag{15}$$

where U_1 and U_2 are determined by

$$U_k = \frac{1}{V}\int_{\mathcal{B}} \Psi_k(x)f(x)dx. \tag{16}$$

The first term in Eq. (15) gives the electrostatic energy change without the pattern on the electric plate, while the second term represents the effect of the pattern on ΔW_e. The coefficient 2 appearing in the pattern effect comes from the condition that the electric plate pattern is present prior to the nanostructure formation.[76]

The detailed derivation procedure of Eqs. (11)–(16), which are valid for the cases of faceted wires and patterns, is presented elsewhere.[77] Interested readers are referred to Refs. 58, 61, 63, and 78–81 for the cases of wavy films and patterns and to Ref. 82 for the case of two piezoelectric solids bonded along a wavy interface.

2. Effects of electrostatic energy on wire formation

Equations (11)–(16) are further explored in this section to understand qualitatively the effects of the electrostatic energy on the wire formation. The discussion starts with the finding that Eq. (14) can be rewritten as

$$\delta W_e = -\int w_e(x)\,\delta v_n d\Gamma, \tag{17}$$

where $d\Gamma$ denotes an area integral and $\delta v_n = \delta f(x)/\sqrt{1+[f'(x)]^2}$ refers to the change of the film morphology in the normal direction **n** pointing out of the film. Equation (17) indicates that the electrostatic energy decreases by w_e when the film surface migrates by one unit length in the normal direction. This suggests the electrostatic energy density w_e is the energetic force associated with the morphological change. Based on this interpretation, the two terms, $2w_{e0}\mathcal{S}\Psi_1(x)$ and $2w_{e0}\mathcal{S}_e\Psi_2(x)$, appearing in the expression for w_e in Eq. (11) can be regarded as the energetic force due to the wire and that due to the pattern on the electric plate, respectively. For conciseness, the former is

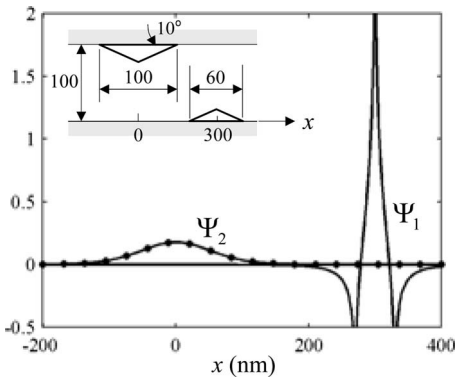

FIG. 3. The variation of $\Psi_1(x)$ and $\Psi_2(x)$ with x for the case where a triangular wire is exposed to an electric plate containing a triangular pattern. The details of the system are depicted in the inset of the figure.

termed the intrinsic energetic force, and the latter is called the extrinsic energetic force.

A typical example of $\Psi_1(x)$ and $\Psi_2(x)$ is depicted in Fig. 3 for the case where a triangular wire is exposed to an electric plate containing a triangular pattern. The electric plate is at a height of 100 nm, the base width of the pattern is 100 nm, that of the wire is 60 nm, the facet angle of both structures is 10°, and the two structures misalign by 300 nm. The result of Ψ_1, corresponding to the intrinsic force for morphological changes, is the highest at the top vertex of the wire and is the lowest at the wire base. The characteristics of Ψ_1 suggest the intrinsic force favors the growth of the wire.

In comparison, the result of Ψ_2 indicates the extrinsic energetic force is the highest at the location right below the tip of the pattern, and the force decays with the distance from the location. The finding suggests the extrinsic force favors wires aligning with the pattern.

Besides the aligning effect, the patterns on the electric plate also affect the size stability of the aligned wire, particularly in the systems where the formation of large wires is suppressed.[83] The pattern effects in those systems depend on the amount of the electrostatic energy reduction induced by the patterns. If the reduction is large, it becomes energetically favorable for large wires to grow in size, leading to coarsening wires. A moderate reduction, on the other hand, is insufficient to trigger the growth of large wires but allows the formation of wires with medium sizes because of the minimum in $\Delta E_I/V$. The difference between the formation of large and medium wires suggests a moderate reduction has the capability to transform an equilibrium flat film into a stable islanded profile. The transformation ceases if the reduction of electrostatic energy is too small.

E. Surface energy and total energy changes

The surface energy change ΔE_s due to the formation of the nanostructure can be expressed as

$$\Delta E_s = \sum_{j=1}^{N} \gamma_0 G_j (b_{j+1} - b_j), \tag{18}$$

where $G_j = -1 + \gamma_j/(\gamma_0 \cos \phi_j)$, γ_j is the surface energy density of the jth facet, and γ_0 is that of the flat wetting layer.

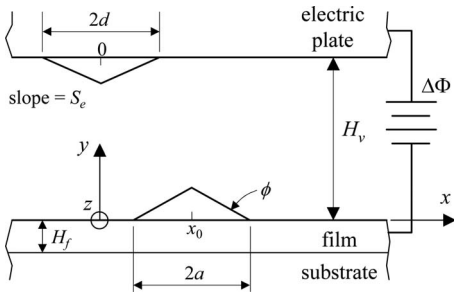

FIG. 4. Schematic diagram of a triangular wire on a SK system under the influence of a triangular pattern on an electric plate with a misalignment of x_0 between the centers of the two structures.

Summing the changes of the strain, electrostatic, interaction, and surface energy yields the total energy change ΔE_{tot},

$$\Delta E_{\text{tot}} = \Delta W_\sigma + \Delta W_e + \Delta E_I + \Delta E_s. \tag{19}$$

III. MODEL AND ENERGY ANALYSIS

This section first presents the model system for analyzing the size stability in Sec. III A. The energy change ΔE_{tot} of the system is then determined in Sec. III B by adopting the formula discussed in Sec. II. The result is further simplified in Sec. III C for the case where the electric plate height is much larger than the wire base width.

A. Model system

Figure 4 plots the model adopted in the paper where a triangular wire on a SK film-substrate system is exposed to an electric plate containing a triangular pattern. The wire is characterized by the slope $\mathcal{S}=\tan\phi$ and the base width $2a$; in comparison, the slope and width of the pattern are $\mathcal{S}_e$ and $2d$, respectively. In addition to the differences in slope and width, the wire and the pattern are also misaligned by x_0. For convenience, the center of the pattern base is taken to be at $(0, H_v)$, and that of the wire at $(x_0, 0)$.

B. Energy analysis

For the triangular wire and pattern considered in the model, the three functions, Ψ_σ, Ψ_1, and Ψ_2, for evaluating the changes of the strain and electrostatic energy can be written down directly by referring to Eqs. (2), (12), and (13),

$$\Psi_\sigma = \frac{2}{\pi} \Re \left[\ln \frac{(x-b_1)(x-b_3)}{(x-x_0)^2} \right], \tag{20}$$

$$\Psi_1 = \frac{1}{\pi} \Re \{ \ln[e^{\eta(x-b_1)} - 1] + \ln[e^{\eta(x-b_3)} - 1] - 2 \ln[e^{\eta(x-x_0)} - 1] \}, \tag{21}$$

$$\Psi_2 = \frac{1}{\pi} \Re \{ \ln[e^{\eta(x+d)} + 1] + \ln[e^{\eta(x-d)} + 1] - 2 \ln[e^{\eta x} + 1] \}, \tag{22}$$

where $b_1 = x_0 - a$ and $b_3 = x_0 + a$. Substituting Eq. (20) into Eq. (5) leads to $U_\sigma = (8 \ln 2)/\pi$; for conciseness, this value is denoted as U_0, i.e.,

$$U_0 = \frac{8}{\pi}\ln 2. \tag{23}$$

Similarly, substituting Ψ_1 and Ψ_2 given in Eqs. (21) and (22) into Eq. (16) yields U_1 and U_2. The quantity U_1 depends on ηa, and U_2 is a function of ηx_0, ηa, and ηd.

After U_σ, U_1, and U_2 are calculated, the total energy change ΔE_{tot} due to the formation of the wire can be determined by substituting Eqs. (4), (10), (15), and (18) into Eq. (19),

$$\Delta E_{\text{tot}} = -w_{\sigma 0}\mathcal{S}VU_0 + 2\gamma_0 Ga - w_{e0}\mathcal{S}VU_1(\eta a) - 2w_{e0}\mathcal{S}_e VU_2(\eta a, \hat{d}, \eta x_0) + \frac{2B}{\sin\phi}\ln\left(\frac{\mathcal{S}a + H_f}{H_f}\right) + \frac{BV}{H_f^2} - \frac{2Ba}{H_f}, \tag{24}$$

where $\hat{d} = d/H_v$, $G = -1 + \gamma/(\gamma_0 \cos\phi)$, and γ is the surface energy density of the wire facet. Equation (24) is the formula used to obtain the numerical results presented in Secs. V and VII.

For moderate values of ηx_0 and ηa, the two quantities U_1 and U_2 have to be evaluated numerically. For the special case where $\eta x_0 \ll 1$ and $\eta a \ll 1$, on the other hand, U_1 and U_2 can be expressed as

$$U_1 = \frac{U_0}{2} + \frac{\eta^2 a^2}{12\pi}, \tag{25}$$

$$U_2 = \mathcal{K}_0 - \frac{\mathcal{K}_2 \eta^2 a^2}{6} - \mathcal{K}_2 \eta^2 x_0^2, \tag{26}$$

where the two constants $\mathcal{K}_0$ and $\mathcal{K}_2$ are given by

$$\mathcal{K}_0 = \frac{2}{\pi}\ln\cosh\frac{\pi\hat{d}}{2},$$

$$\mathcal{K}_2 = \frac{1}{4\pi}\left(1 - \cosh^{-2}\frac{\pi\hat{d}}{2}\right). \tag{27}$$

The quantity U_1 given in Eq. (25) refers to the effect of the wire shape on ΔW_e when $\eta a \ll 1$. The result is found to be positive, meaning the electrostatic energy is reduced when the wire is formed.

The quantity U_2 expressed in Eq. (26) consists of three terms. The first two terms represent the pattern shape effect on ΔW_e, and the sum of the two terms is positive since $\mathcal{K}_0 > 0$ and $\eta a \ll 1$. This proves our earlier contention in Sec. II D that the pattern on the electric plate enhances the electrostatic energy reduction during the wire formation. The third term of U_2 corresponds to the misalignment effect on ΔW_e; this term is always negative, which means the electrostatic energy of a misaligned wire is higher than that of an aligned one with the same amount of volume. The finding is consistent with the result of $\Psi_2(x)$ illustrated in Fig. 3.

Substituting the results of U_1 and U_2 given in Eqs. (25) and (26) into Eq. (24) and taking $x_0 = 0$ yields ΔE_{tot} of aligned wires under the condition $\eta a = \pi a/H_v \ll 1$. The result can be further reduced to the following concise form by adopting the simplification that $\sin\phi \approx \mathcal{S}$,

$$\Delta E_{\text{tot}} = -w_{\sigma 0}\mathcal{S}VU_0 + 2\gamma_0 Ga - \frac{1}{2}w_{e0}\mathcal{S}VU_0 - 2w_{e0}\mathcal{S}_e V\mathcal{K}_0 - \frac{w_{e0}\eta^2 V^2}{12\pi\mathcal{S}} + \frac{w_{e0}\mathcal{S}_e\mathcal{K}_2\eta^2 V^2}{3\mathcal{S}} + \frac{2B}{\mathcal{S}}\ln\left(\frac{\mathcal{S}a + H_f}{H_f}\right) + \frac{BV}{H_f^2} - \frac{2Ba}{H_f}. \tag{28}$$

Equation (28) is the starting point for the stability analyses presented in Secs. IV and VI.

C. Parameters and normalization

Before normalizing ΔE_{tot} expressed in Eq. (28), it is helpful to introduce three key parameters of the EMSO process, namely, the normalized film thickness $\hat{H}_f$, the normalized stability number $\hat{\Sigma}$, and the electromolding (EM) strength $\mathcal{J}$. The three parameters dominate the characteristics of the total energy change and the size stability of the wire.

The normalized film thickness $\hat{H}_f$ is defined to be

$$\hat{H}_f = \frac{H_f}{H_1}, \tag{29}$$

where H_1 is the critical thickness for spontaneous island formation (or called the first critical thickness in the literature),[45]

$$H_1 = \sqrt{\frac{BL}{\gamma_0 U_0 \mathcal{S}}}. \tag{30}$$

The quantity $L = \gamma_0/w_{\sigma 0}$ in Eq. (30) gives the length scale at which the strain energy reduction due to the wire formation is balanced by the corresponding surface energy increment.

The normalized stability number $\hat{\Sigma}$ is given by[10]

$$\hat{\Sigma} = \frac{1}{G}\sqrt{\frac{BU_0\mathcal{S}}{\gamma_0 L}} - 1. \tag{31}$$

A positive value of $\hat{\Sigma}$ means that the SK system can develop an island array that is stable against coarsening, while a negative value indicates the opposite. Since G is positive for the SK systems, the parameter $\hat{\Sigma}$ is larger than -1.

The EM strength $\mathcal{J}$ is expressed as

$$\mathcal{J} = 1 + \frac{1}{2}\hat{w}_{e0} + 2\hat{w}_{e0}\hat{\mathcal{S}}_e\frac{\mathcal{K}_0}{U_0}, \tag{32}$$

where $\hat{w}_{e0} = w_{e0}/w_{\sigma 0}$ and $\hat{\mathcal{S}}_e = \mathcal{S}_e/\mathcal{S}$. The parameter $\mathcal{J}$, depending on $\hat{w}_{e0}$, $\hat{\mathcal{S}}_e$, and $\hat{d}$, describes the effect of the electric field on ΔE_{tot} when $\eta a \ll 1$ and $x_0 = 0$. The variation of $\mathcal{J}$ with $\hat{d}$ and $\hat{\mathcal{S}}_e$ is plotted in Fig. 5 for the case where $\hat{w}_{e0} = 0.5$. The result indicates $\mathcal{J}$ increases with $\hat{d}$ and $\hat{\mathcal{S}}_e$.

In addition to $\hat{H}_f$, $\hat{\Sigma}$, and $\mathcal{J}$, the total energy change ΔE_{tot} is also affected by the parameter $\mathcal{J}_2 = -\pi\hat{w}_{e0}\hat{H}_f^4(1$

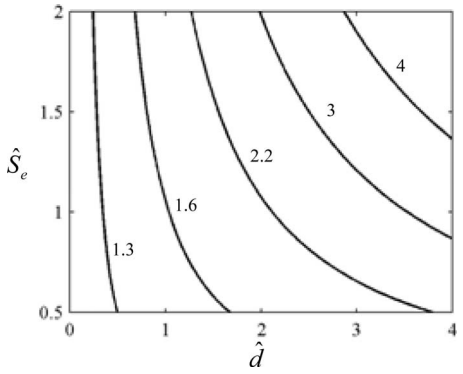

FIG. 5. The contours of $\mathcal{J}$ as a function of $\hat{d}$ and $\hat{\mathcal{S}}_e$ for the case where $\hat{w}_{e0}=0.5$.

$-4\pi\hat{\mathcal{S}}_e\mathcal{K}_2)/(24U_0\mathcal{S}^2)$. Though influencing ΔE_{tot}, this parameter has little effect on the condition of the wire size stability, as shown later in Sec. VI.

By evoking the definitions of $\hat{H}_f$, $\hat{\Sigma}$, $\mathcal{J}$, and $\mathcal{J}_2$, the total energy change ΔE_{tot} expressed in Eq. (28) can be rewritten as

$$\Delta\hat{E}_{\text{tot}} = \ln(1+\hat{a}) + \hat{c}_1\hat{a} + \hat{c}_2\hat{a}^2 + \hat{c}_4\hat{a}^4, \tag{33}$$

where $\Delta\hat{E}_{\text{tot}}=\mathcal{S}\Delta E_{\text{tot}}/(2B)$, $\hat{a}=\mathcal{S}a/H_f$, and the three coefficients, $\hat{c}_1$, $\hat{c}_2$, and $\hat{c}_4$, are given by

$$\hat{c}_1 = \frac{\hat{H}_f - 1 - \hat{\Sigma}}{1+\hat{\Sigma}}, \tag{34}$$

$$\hat{c}_2 = \frac{1}{2}(1 - \mathcal{J}\hat{H}_f^2), \tag{35}$$

$$\hat{c}_4 = \frac{\mathcal{J}_2 H_1^2}{H_v^2}. \tag{36}$$

It is found that $\hat{c}_1$ and $\hat{c}_2$ are fully controlled by $\hat{H}_f$, $\hat{\Sigma}$, and $\mathcal{J}$, and $\hat{c}_4$ is proportional to H_v^{-2} as $H_v \to \infty$.

IV. SK SYSTEMS WITHOUT ELECTRIC FIELD

As a first step, this section focuses on the SK systems without an electric field. Of particular interest is the condition under which the systems can form a wire stable against size variation. The results of this special case are used as a reference point for those under the influence of an electric field.

A. Characteristics of the total energy change

When the electric field is absent from the system, $w_{e0}=0$, $\mathcal{J}=1$, $\hat{c}_4=0$, and the total energy change ΔE_{tot} expressed in Eq. (33) is reduced to

$$\Delta\hat{E}_{\text{tot}} = \ln(1+\hat{a}) + \hat{c}_1\hat{a} + \hat{c}_2^*\hat{a}^2, \tag{37}$$

where $\hat{c}_1$ is given in Eq. (34) and $\hat{c}_2^*=(1-\hat{H}_f^2)/2$.

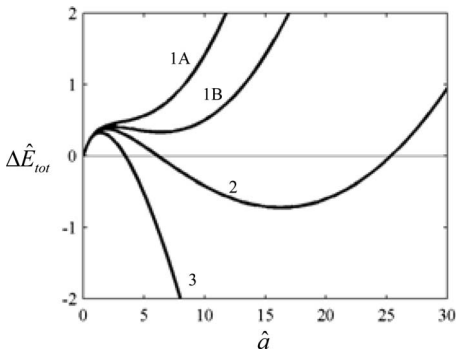

FIG. 6. The variation of $\Delta\hat{E}_{\text{tot}}$ with $\hat{a}$ for the cases where $\hat{\Sigma}=0.6$ and $\hat{H}_F=0.97$, 0.98, 0.99, and 1.02, which are denoted by lines 1A, 1B, 2, and 3, respectively.

The variation of $\Delta\hat{E}_{\text{tot}}$ with $\hat{a}$ is plotted in Fig. 6 for the cases where $\hat{\Sigma}=0.6$ and $\hat{H}_f=0.97$, 0.98, 0.99, and 1.02. The results are denoted by lines 1A, 1B, 2, and 3, respectively. Lines 1A, 1B, and 2 describe typical examples of $\Delta\hat{E}_{\text{tot}}$ when $\hat{H}_f<1$, and line 3 illustrates $\Delta\hat{E}_{\text{tot}}$ when $\hat{H}_f>1$. These lines have the same property that the slope $d\Delta\hat{E}_{\text{tot}}/d\hat{a}$ is positive at $\hat{a}=0$, while they differ in the maximum and minimum points of $\Delta\hat{E}_{\text{tot}}(\hat{a})$: Line 1A shows a monotonic increase in $\Delta\hat{E}_{\text{tot}}$ with $\hat{a}$, line 1B is distinguished by a maximum and a positive minimum of $\Delta\hat{E}_{\text{tot}}$, line 2 is similar to line 1B but the minimum is negative, and line 3 is characterized by a maximum point followed by a monotonic decrease in $\Delta\hat{E}_{\text{tot}}$.

These characteristics of $\Delta\hat{E}_{\text{tot}}(\hat{a})$ signify different types of film morphology. In particular, lines 1A and 1B indicate $\Delta\hat{E}_{\text{tot}}$ is the lowest at $\hat{a}=0$, meaning the wire cannot form and the flat film is the equilibrium morphology. The negative minimum on line 2, on the other hand, suggests the system can develop a wire stable against size variation. Wires can also form in the case of line 3 since $\Delta\hat{E}_{\text{tot}}$ can be negative; however, the lack of a minimum on line 3 means the wires are unstable in this case.

In brief, the film can be classified into three types of morphology, namely, the unstable wire, the stable wire, and the stable flat film. The unstable wire develops when $\hat{H}_f>1$. The stable wire and the stable flat film, on the other hand, occur in the thickness range $\hat{H}_g<1$; the condition differentiating the two types of morphology is further investigated in Sec. IV B.

B. Stability condition against size variation

The results depicted in Fig. 6 suggest that the film morphology is characterized by the stable wire when the following two conditions are satisfied:

(a) Condition I—There are one maximum and one minimum points in $\Delta\hat{E}_{\text{tot}}$.

(b) Condition II—The minimum of $\Delta\hat{E}_{\text{tot}}$ is negative.

The key quantities in the stable-wire conditions are the minimum/maximum points of $\Delta\hat{E}_{\text{tot}}$, which can be derived by solving the equation $\Delta\hat{E}_{\text{tot}}/d\hat{a}=0$,

$$\hat{a}_1 = \frac{-(2\hat{c}_2^* + \hat{c}_1) - \sqrt{Q}}{4\hat{c}_2^*}, \tag{38}$$

$$\hat{a}_2 = \frac{-(2\hat{c}_2^* + \hat{c}_1) + \sqrt{Q}}{4\hat{c}_2^*}, \tag{39}$$

where $2\hat{c}_2^* + \hat{c}_1$ and Q are functions of $\hat{\Sigma}$ and $\hat{H}_f$,

$$2\hat{c}_2^* + \hat{c}_1 = \frac{\hat{H}_f}{1+\hat{\Sigma}}[1-(1+\hat{\Sigma})\hat{H}_f], \tag{40}$$

$$Q = (2\hat{c}_2^* + \hat{c}_1)^2 - 8(1+\hat{c}_1)\hat{c}_2^*$$
$$= \frac{\hat{H}_f}{1+\hat{\Sigma}}[(1+\hat{\Sigma})^2\hat{H}_f^3 + 2(1+\hat{\Sigma})\hat{H}_f^2 + \hat{H}_f - 4(1+\hat{\Sigma})]. \tag{41}$$

If both $\hat{a}_1$ and $\hat{a}_2$ are positive numbers, the two solutions correspond to the maximum and minimum points of $\Delta\hat{E}_{\text{tot}}$, respectively, meaning condition I is satisfied. In contrast, if any one of $\hat{a}_1$ and $\hat{a}_2$ is a negative or complex number, there is no minimum point in $\Delta\hat{E}_{\text{tot}}$ and condition I cannot be met.

The criterion of positive $\hat{a}_1$ and $\hat{a}_2$ holds in the overlapping regime of the following three domains:

$$Q > 0, \tag{42}$$

$$2\hat{c}_2^* + \hat{c}_1 < 0, \tag{43}$$

$$\hat{c}_2^* > 0. \tag{44}$$

The first domain described by Eq. (42) ensures that $\hat{a}_1$ and $\hat{a}_2$ are real numbers, and the remaining two domains enforce $\hat{a}_1$ and $\hat{a}_2$ to be positive.

The three domains are plotted in Fig. 7(a) to determine the regime of $(\hat{\Sigma}, H_f)$ that satisfies condition I. The results clearly show that condition I cannot be satisfied for SK systems with $\hat{\Sigma} < 0$. For SK systems with $\hat{\Sigma} > 0$, on the contrary, condition I is met if the normalized film thickness $\hat{H}_f$ falls into the range $[\hat{H}_Q, 1]$, where $\hat{H}_Q$ is the solution to the equation $Q(\hat{H}_Q, \hat{\Sigma}) = 0$. The critical thickness $\hat{H}_Q$ for condition I is equal to 1 at $\hat{\Sigma} = 0$ and decreases with increasing $\hat{\Sigma}$; see Fig. 7(a).

Calculating the minimum of $\Delta\hat{E}_{\text{tot}}$ in the thickness range $[\hat{H}_Q, 1]$ indicates the minimum $\Delta\hat{E}_{\text{min}}$ is always positive at $\hat{H}_f = \hat{H}_Q$, decreases gradually as $\hat{H}_f$ increases, and becomes zero at the thickness $\hat{H}_E$. The variation of $\hat{H}_E$ with $\hat{\Sigma}$ is plotted in Fig. 7(b). Similar to $\hat{H}_Q$, $\hat{H}_E$ is equal to 1 at $\hat{\Sigma} = 0$ and decreases as $\hat{\Sigma}$ increases. The domain between $\hat{H}_f = 1$ and $\hat{H}_f = \hat{H}_E(\hat{\Sigma})$ gives the regime of $(\hat{\Sigma}, \hat{H}_f)$ that satisfies conditions I and II for stable wires.

C. Summary of SK systems without electric field

In summary, the dependence of the wire stability on the two parameters $\hat{\Sigma}$ and $\hat{H}_f$ of the SK systems can be illustrated by the phase diagram shown in Fig. 7(b). The diagram is divided into three regimes along the two boundaries, $\hat{H}_f = 1$ and $\hat{H}_f = \hat{H}_E$. In the regime above the boundary $\hat{H}_f = 1$, the total energy change $\Delta\hat{E}_{\text{tot}}$ is described by line 3 in Fig. 6, which shows $\Delta\hat{E}_{\text{tot}}$ decreases with $\hat{a}$ when $\hat{a}$ is sufficiently large. This characteristic means the strain energy reduction is higher than the volume contribution of the interaction energy, and the wires are unstable against coarsening.

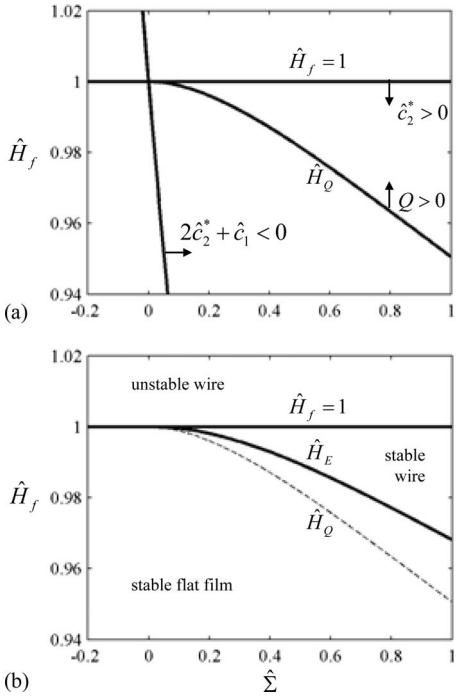

FIG. 7. (a) The regime of $(\hat{\Sigma}, \hat{H}_F)$ satisfying condition I; (b) the phase diagram of the film morphology of the SK systems without an electric field.

Turn to the regime between the two boundaries, which can also be expressed as $\hat{H}_E < \hat{H}_f < 1$. The inequality $\hat{H}_f < 1$ ensures that the strain energy reduction is less than the volume contribution of the interaction energy; accordingly, the growth of large wires is suppressed. The inequality $\hat{H}_E < \hat{H}_f$, on the other hand, requires that the formation of wires of moderate size is still energetically favorable in spite of the suppression of large wires. The difference between the growth of large and moderate wires results in the size stability. The total energy change $\Delta\hat{E}_{\text{tot}}(\hat{a})$ of this case is represented by line 2 in Fig. 6.

The regime below both boundaries refers to a stable flat film, and the total energy change is described by line 1A or 1B in Fig. 6.[84] In this regime the volume contribution of the interaction energy far exceeds the strain energy reduction, suppressing the formation of any wire.

V. ELECTRIC FIELD EFFECTS ON ALIGNED WIRES

This section adopts a typical coarsening system as an example to investigate the effects of H_v and d on the size stability of wires that align with the patterns. The results

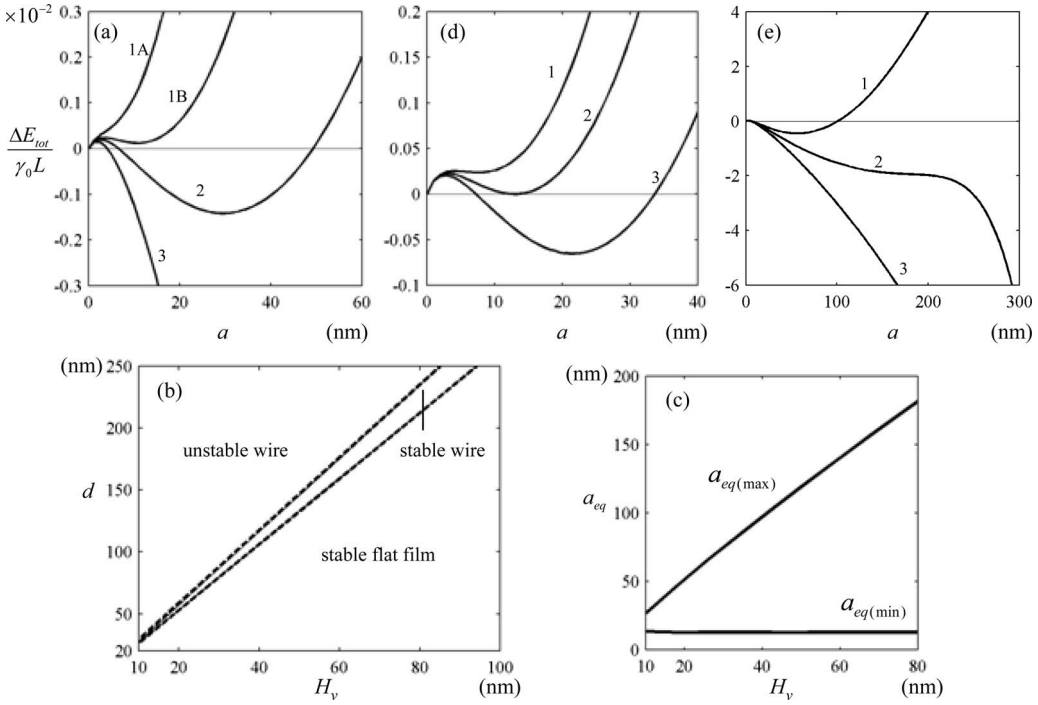

FIG. 8. (a) The variation of $\Delta E_{\text{tot}}/\gamma_0 L$ with a for the cases where $H_v=50$ nm and $d=110$, 131, 140, and 160 nm, denoted by lines 1A, 1B, 2, and 3, respectively. (b) The domains of (d,H_v) that lead to a stable flat film, a stable wire, and an unstable wire. (c) The variation of the stable-wire sizes $a_{\text{eq(min)}}$ and $a_{\text{eq(max)}}$ with the electric plate height H_v. (d) The variation of $\Delta E_{\text{tot}}/\gamma_0 L$ with a for the cases where $H_v=80$ nm and d is in the vicinity of the lower boundary of the stable-wire regime; $d=205$, 212.4, and 220 nm for lines 1, 2, and 3, respectively. (e) The variation of $\Delta E_{\text{tot}}/\gamma_0 L$ with a for the cases where $H_v=80$ nm and d is in the vicinity of the upper boundary; $d=230$, 235, and 240 nm for lines 1, 2, and 3, respectively. The parameters adopted in the calculation are listed as follows: $L=100$ nm, $\gamma_0=1$ J/m^2, $\gamma=0.99$ J/m^2, $B=1.5\times10^{-11}$ J/m, $\mathcal{S}=\mathcal{S}_e=1/5$, $\hat{w}_{e0}=3$, and $\hat{H}_f=0.3$. The normalized stability number $\hat{\Sigma}$ can be evaluated to be -0.24.

demonstrate the potential of using a patterned electric plate to fabricate stable wires. The results also reveal interesting features that motivate further stability analyses of the case where H_v and d are large in Sec. VI.

A. Characteristics of ΔE_{tot} and phase diagram of wire size stability

The size stability is determined by employing Eq. (24) to evaluate $\Delta E_{\text{tot}}(a)$ for different values of H_v and d. Typical examples of $\Delta E_{\text{tot}}(a)$ are depicted in Fig. 8(a) where $H_v=50$ nm and $d=110$, 131, 140, and 160 nm. The results are found to be similar to those in Fig. 6 for the case without an electric field. The finding suggests the SK systems under the influence of an electric field can still be classified into the three types of film morphology discussed in Sec. IV, namely, a stable flat film, a stable wire, and an unstable wire.

The dependence of the film morphology on H_v and d is summarized by the phase diagram shown in Fig. 8(b). The diagram indicates stable flat films happen at small d and large H_v, unstable wires are triggered at large d and small H_v, and stable wires are obtained in the regime between the two solid lines shown in the phase diagram. (The dashed boundaries in the diagram are discussed later in Sec. V B.) The existence of the stable-wire regime demonstrates that the EMSO process can cause an originally coarsening SK system to develop wires stable against size variation.

The stable-wire regime implies, for given electric plate height H_v, a range of pattern size d can be adopted to generate stable wires of different sizes. For example, taking d to be the value $d_{\max}$ on the upper boundary of the stable-wire regime results in the largest stable-wire size $a_{\text{eq(max)}}$, while adopting $d_{\min}$ on the lower boundary yields the smallest stable-wire size $a_{\text{eq(min)}}$. The size range $[a_{\text{eq(min)}},a_{\text{eq(max)}}]$ of the stable wires is plotted in Fig. 8(c) as a function of H_v. The results show $a_{\text{eq(max)}}$ increases with H_v, while $a_{\text{eq(min)}}$ is insensitive to the electric plate height H_v.

B. Boundaries of stable-wire regime

After discussing the phase diagram of size stability and the effect of H_v on the range of stable-wire size, the focus of this section turns to the two boundaries of the stable-wire regime in the phase diagram. The lower boundary is examined in Fig. 8(d) by depicting $\Delta E_{\text{tot}}(a)$ of three cases where the values of d are in the vicinity of the lower boundary and H_v is fixed. In particular, line 1 plots ΔE_{tot} when d is lower than the value $d_{\min}$ on the boundary, line 2 illustrates the result of the case where $d=d_{\min}$, and line 3 presents that when $d>d_{\min}$. The results indicate two properties of the lower boundary. First, the lower boundary is determined by the condition that the minimum of ΔE_{tot} is equal to zero. Second, the lower boundary signifies the onset of the morphological transition from a stable flat film to a stable wire.

The morphological transition happens when the electric field effect caused by the patterned electrode is sufficiently strong.

Similarly, the upper boundary is investigated in Fig. 8(e) by considering the cases where d are lower than, equal to, and higher than the value $d_{\max}$ on the upper boundary. The results, denoted by lines 1, 2, and 3, respectively, demonstrate that the upper boundary corresponds to the morphological transition from a stable to an unstable wire, and is characterized by the scenario that the curvature of the minimum point of ΔE_{tot} vanishes.

The lower and upper boundaries generally have to be determined by numerical methods, preventing the two boundaries from being described analytically. Further examination of the example depicted in Fig. 8(b), however, reveals that the two boundaries of the stable-wire regime approach straight lines at large values of d and H_v. The straight lines are expressed as $d=\alpha H_v$ (α is a constant), and are denoted by the dashed boundaries in the phase diagram. Motivated by the simple expression for the boundaries of the stable-wire regime, we investigate the wire size stability of the asymptotic cases in Sec. VI.

VI. ASYMPTOTIC CASES

The size stability of the asymptotic case is analyzed by considering the onset of two critical morphological transitions, namely, the flat film–stable wire transition and the stable-unstable wire transition. The former is studied in Sec. VI A, yielding the minimum criterion for the EM strength. The latter, imposing an upper limit on the EM strength, is investigated in Sec. VI B. The results of the two sections are summarized in Sec. VI C to present an overall picture of the asymptotic cases. For convenience, the onset of the flat film–stable wire transition is termed the basic stable state, while that of the stable-unstable wire transition is called the utmost stable state.

A. Minimum criterion and basic stable states

1. Derivation of the basic stable states

The asymptotic cases are characterized by the condition that the height H_v and the pattern size d are large. This implies $\eta a=\pi a/H_v \ll 1$, and the total energy change $\Delta\hat{E}_{\text{tot}}$ can be expressed by Eq. (33). The expression can be further simplified by neglecting the term $\hat{c}_4\hat{a}^4$ when studying the basic stable states since Eqs. (34)–(36) and Fig. 8(c) suggest $\hat{c}_1$, $\hat{c}_2$, and $\hat{a}$ of the basic stable states are invariant with H_v, but $\hat{c}_4 \to 0$ as H_v approaches infinity. The simplification leads $\Delta\hat{E}_{\text{tot}}$ to

$$\Delta\hat{E}_{\text{tot}} = \ln(1+\hat{a}) + \hat{c}_1\hat{a} + \hat{c}_2\hat{a}^2, \tag{45}$$

where $\hat{c}_1$ is a function of $\hat{H}_f$ and $\hat{\Sigma}$, and $\hat{c}_2$ is that of $\hat{H}_f$, $\hat{\Sigma}$, and the EM strength $\mathcal{J}$.

Differentiating Eq. (45) with respect to $\hat{a}$ and requiring the result to be zero yield an equation for the wire size $\hat{a}_{\min}$ at the minimum point,

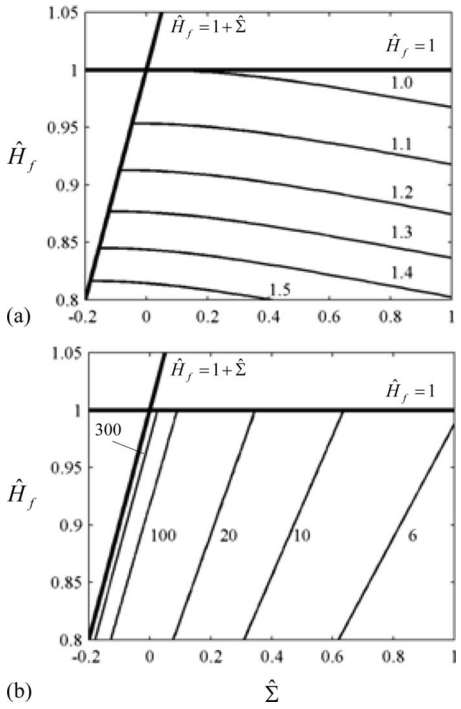

FIG. 9. The contours of (a) $\mathcal{J}_{\min}$ and (b) $\hat{a}_{\min}$ of the basic stable states as functions of $\hat{\Sigma}$ and $\hat{H}_f$.

$$\frac{1}{1+\hat{a}_{\min}}[2\hat{c}_2\hat{a}_{\min}^2 + (\hat{c}_1+2\hat{c}_2)\hat{a}_{\min} + 1 + \hat{c}_1] = 0. \tag{46}$$

The minimum point is a basic stable state if the total energy change is zero at that point,

$$\ln(1+\hat{a}_{\min}) + \hat{c}_1\hat{a}_{\min} + \hat{c}_2\hat{a}_{\min}^2 = 0. \tag{47}$$

Equations (46) and (47) constitute the conditions of the basic stable states.

By evoking the definitions of $\hat{c}_1$ and $\hat{c}_2$ given in Eqs. (34) and (35), the two conditions for the basic stable states can be rewritten in terms of $\hat{H}_f$, $\hat{\Sigma}$, $\hat{a}_{\min}$, and $\mathcal{J}_{\min}$, where $\mathcal{J}_{\min}$ denotes the EM strength of the basic stable states. Among the four variables, $\hat{H}_f$ and $\hat{\Sigma}$ are known for a given SK system. Substituting the values of $\hat{H}_f$ and $\hat{\Sigma}$ into the conditions yields two equations for determining $\mathcal{J}_{\min}$ and $\hat{a}_{\min}$ of the basic stable states. The two equations can be solved numerically.

2. Viable regime

The EM strength $\mathcal{J}_{\min}$ and the normalized wire size $\hat{a}_{\min}$ of the basic stable states are depicted in Figs. 9(a) and 9(b), respectively, as functions of $\hat{\Sigma}$ and $\hat{H}_f$. The results indicate both $\mathcal{J}_{\min}$ and $\hat{a}_{\min}$ can be obtained in the overlapping regime of the following two domains:

$$\hat{H}_f < 1,$$

$$\hat{H}_f < 1+\hat{\Sigma}. \tag{48}$$

The overlapping regime identifies the SK systems that can be activated by the EMSO process to develop wires stable

against size variation, and is termed the viable regime. For SK systems out of the viable regime, the conditions of the basic stable states cannot be satisfied for any value of $\mathcal{J}_{\min}$ and $\hat{a}_{\min}$. Those systems are characterized by coarsening wires ($\hat{H}_f > 1$) or stable flat films ($1+\hat{\Sigma} < \hat{H}_f < 1$).

The viable regime illustrated in Fig. 9 suggests that all of the noncoarsening SK systems ($\hat{\Sigma} > 0$) with $\hat{H}_f < 1$ can develop stable wires during the EMSO process. This is in contrast to the case without an electric field where the stable states can only occur in a much smaller thickness range $[\hat{H}_E(\hat{\Sigma}), 1]$. In addition to the noncoarsening systems, the viable regime also includes the coarsening systems with $\hat{H}_f$ less than $1+\hat{\Sigma}$.

3. Minimum EM strength $\mathcal{J}_{\min}$

The EM strength of the basic stable states, denoted as $\mathcal{J}_{\min}$, is the minimum EM strength needed in order to induce a stable wire for the given values of $\hat{H}_f$ and $\hat{\Sigma}$.[85] When the EM strength is less than $\mathcal{J}_{\min}$, the electrostatic energy reduction due to the patterned electric plate is insufficient to cause the formation of wires; as a consequence, the flat film is the equilibrium morphology [see line 1 in Fig. 8(d)]. Increasing the EM strength $\mathcal{J}$ leads to higher electrostatic energy reduction. When $\mathcal{J}$ exceeds $\mathcal{J}_{\min}$, the wire formation becomes energetically favorable for wires with moderate size [see line 3 in Fig. 8(d)]. This implies stability against size variation.

The minimum EM strength $\mathcal{J}_{\min}$ depends on two parameters, namely, $\hat{H}_f$ and $\hat{\Sigma}$. The variation of $\mathcal{J}_{\min}$ with the two parameters is depicted in Fig. 9(a). The results show that $\mathcal{J}_{\min}$ decreases when $\hat{\Sigma}$ and/or $\hat{H}_f$ increases.

Figure 9(a) indicates the minimum EM strength $\mathcal{J}_{\min}$ is less than 1 in the area between the contour $\mathcal{J}_{\min}=1$ and the line $\hat{H}_f=1$. Since the $\mathcal{J} \geq 1$, the inequality $1 > \mathcal{J}_{\min}$ means the condition $\mathcal{J} > \mathcal{J}_{\min}$ for size stability is always satisfied in the area, and the corresponding SK systems can develop stable wires even if $\hat{w}_{e0}=0$. The finding shows that the area is actually the stable-wire regime illustrated in Fig. 7(b) for SK systems without an electric field,[86] and the boundary $\mathcal{J}_{\min}(\hat{H}_f, \hat{\Sigma})=1$ of the area is equivalent to the line $\hat{H}_f = \hat{H}_E(\hat{\Sigma})$ defined in Fig. 7(b).

4. Wire size of basic stable states

Turn to $\hat{a}_{\min}$, the wire size of the basic stable states and the smallest size of the stable wires in the asymptotic cases. As discussed earlier in this section, $\hat{a}_{\min}$ can be obtained by solving Eqs. (46) and (47) with given $\hat{\Sigma}$ and $\hat{H}_f$. This shows $\hat{a}_{\min}$ is fully controlled by $\hat{\Sigma}$ and $\hat{H}_f$ of the SK systems, independent of the electric field generated by the patterned electrode. The result explains the finding in Fig. 8(c) that the smallest stable-wire size $a_{\text{eq(min)}}$ is insensitive to the electric plate height H_v.

The effects of $\hat{\Sigma}$ and $\hat{H}_f$ on the wire size $\hat{a}_{\min}$ of the basic stable states are depicted in Fig. 9(b). The results indicate $\hat{a}_{\min}$ decreases when $\hat{\Sigma}$ is raised or $\hat{H}_f$ is reduced, while $\hat{a}_{\min}$ increases drastically when approaching the boundary $\hat{H}_f = 1+\hat{\Sigma}$ of the viable regime. The wire size $\hat{a}_{\min}$ in the vicinity of the boundary is further explored in the Appendix.

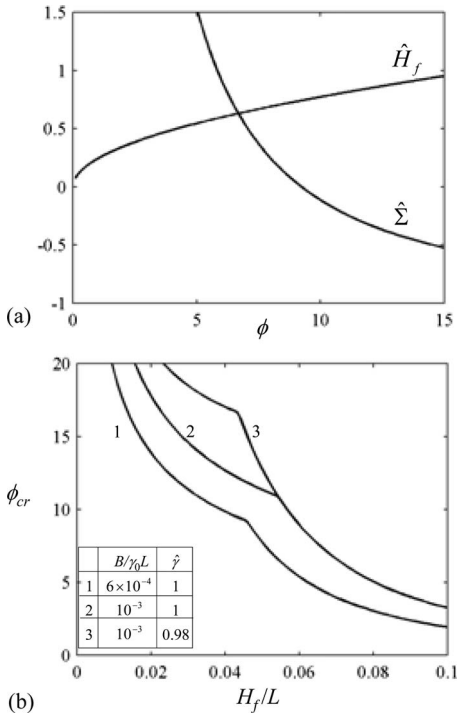

FIG. 10. (a) The variation of $\hat{H}_f$ and $\hat{\Sigma}$ with ϕ for the case where $B=1.5\times10^{-11}$ J/m, $L=25$ nm, $H_f=1.5$ nm, and $\gamma_0=\gamma=1$ J/m^2. (b) The variation of ϕ_{cr} with $\hat{H}_f/L$ of three cases: $B/\gamma_0 L=6\times10^{-4}$ and $\hat{\gamma}=1$ for line 1, $B/\gamma_0 L=10^{-3}$ and $\hat{\gamma}=1$ for line 2, and $B/\gamma_0 L=10^{-3}$ and $\hat{\gamma}=0.98$ for line 3.

5. Effects of facet angle ϕ

Figure 9 can be employed to understand the effects of the facet angle ϕ on the wire size stability. As an example, consider the case where $B=1.5\times10^{-11}$ J/m, $L=25$ nm, $H_f=1.5$ nm, and $\gamma_0=\gamma=1$ J/m^2. Substituting these values into Eqs. (29) and (31) determines the variation of $\hat{H}_f$ and $\hat{\Sigma}$ with the facet angle ϕ; see Fig. 10(a). The results indicate $\hat{H}_f$ increases with ϕ, while $\hat{\Sigma}$ decreases with the facet angle. The changes of $\hat{H}_f$ and $\hat{\Sigma}$, according to Fig. 9(a), would cause the SK system to be outside the viable regime. This demonstrates that the nanostructures are unstable against size variation when the facet angle is sufficiently high.

The critical facet angle ϕ_{cr} for stable-wire size is controlled by H_f/L, $B/\gamma_0 L$, and $\hat{\gamma}=\gamma/\gamma_0$. The variation of ϕ_{cr} with H_f/L is illustrated by line 1 of Fig. 10(b) for the case where $B/\gamma_0 L=6\times10^{-4}$ and $\hat{\gamma}=1$. The line consists of two smooth curves. The curve at small values of H_f/L corresponds to ϕ at the boundary $\hat{H}_f=1+\hat{\Sigma}$ of the viable regime, which depends on $B/\gamma_0 L$ and $\hat{\gamma}$. In comparison, the curve at large H_f/L corresponds to ϕ at the other boundary $\hat{H}_f=1$, which is dictated by $B/\gamma_0 L$. On both curves, ϕ_{cr} decreases with $\hat{H}_f/L$.

In addition to line 1, Fig. 10(b) also depicts the variation of ϕ_{cr} with H_f/L for another two cases to show the depen-

dence of ϕ_{cr} on $B/\gamma_0 L$ and $\hat{\gamma}$. In particular, line 2 considers the case where $\hat{\gamma}$ remains the same but $B/\gamma_0 L$ is raised to 10^{-3}, while line 3 adopts $B/\gamma_0 L = 10^{-3}$ and reduces $\hat{\gamma}$ to 0.98. The comparison between lines 1 and 2 demonstrates that ϕ_{cr} is increased when $B/\gamma_0 L$ is enhanced. The comparison between lines 2 and 3 suggests lowering $\hat{\gamma}$ also causes ϕ_{cr} to increase. The effect of $\hat{\gamma}$, however, diminishes as $\hat{H}_f/L$ increases.

B. Utmost stable states and maximum EM strength $\mathcal{J}_{\max}$

1. Utmost stable states

This section first focuses on the utmost stable state under the condition $\hat{c}_4 < 0$, which is satisfied when $\hat{\mathcal{S}}_e < 1$. It is then shown that the result is also applicable to the cases with $\hat{c}_4 > 0$.

The utmost stable states, as illustrated in Fig. 8(e), are characterized by a stationary point with zero curvature in $\Delta\hat{E}_{\text{tot}}$ to signify the onset of no minimum in the total energy change. The characteristic can be described by the two equations, $\Delta\hat{E}'_{\text{tot}}(\hat{a}_{\max}) = \Delta\hat{E}''_{\text{tot}}(\hat{a}_{\max}) = 0$. By assuming $\hat{c}_4 < 0$, the two equations can be expressed as

$$\frac{1}{1+\hat{a}_{\max}} + \hat{c}_1 + 2\hat{c}_2\hat{a}_{\max} + 4\hat{c}_4\hat{a}_{\max}^3 = 0, \tag{49}$$

$$-\frac{1}{(1+\hat{a}_{\max})^2} + 2\hat{c}_2 + 12\hat{c}_4\hat{a}_{\max}^2 = 0, \tag{50}$$

where $\hat{a}_{\max}$ is the wire size of the utmost stable state. Comparing the order of magnitude of the terms in Eqs. (49) and (50) suggests $(1+\hat{a}_{\max})^{-1}$ and $(1+\hat{a}_{\max})^{-2}$ can be neglected, simplifying the two equations to

$$\hat{c}_1 + 2\hat{c}_2\hat{a}_{\max} + 4\hat{c}_4\hat{a}_{\max}^3 = 0, \tag{51}$$

$$2\hat{c}_2 + 12\hat{c}_4\hat{a}_{\max}^2 = 0. \tag{52}$$

Equations (51) and (52) can be solved to express $\hat{c}_2$ and $\hat{a}_{\max}$ in terms of $\hat{c}_1$ and $\hat{c}_4$,

$$\hat{a}_{\max} = \left(\frac{\hat{c}_1}{8\hat{c}_4}\right)^{1/3}, \tag{53}$$

$$\hat{c}_2 = -\frac{3\hat{c}_1}{4\hat{a}_{\max}}. \tag{54}$$

Since $\hat{c}_4$ is proportional to H_v^{-2} when H_v approaches infinity, Eqs. (53) and (54) imply $\hat{a}_{\max} \propto H_v^{2/3}$ and $\hat{c}_2 \propto H_v^{-2/3}$. The result $\hat{a}_{\max} \propto H_v^{2/3}$ confirms the insignificance of $(1+\hat{a}_{\max})^{-1}$ and $(1+\hat{a}_{\max})^{-2}$ in Eqs. (49) and (50), respectively. The finding $\hat{c}_2 \propto H_v^{-2/3}$ suggests the EM strength of the utmost stable states is given by

$$\mathcal{J}_{\max} = \frac{1}{\hat{H}_f^2}. \tag{55}$$

For the case where $\hat{c}_4 > 0$, it is necessary to include higher order terms of $\hat{a}$ in order to determine the maximum stable size $\hat{a}_{\max}$. The EM strength, however, is still given by Eq. (55) because the coefficients of the higher order terms, similar to $\hat{c}_4$, all decay to zero as $H_v \to \infty$. In such a case, the minimum point of $\Delta\hat{E}_{\text{tot}}$ would cease to exist when $\hat{c}_2 \leq 0$. The critical condition $\hat{c}_2 = 0$ leads to the result expressed in Eq. (55).

2. Maximum EM strength $\mathcal{J}_{\max}$

The EM strength $\mathcal{J}_{\max}$ at the utmost stable state is the maximum EM strength allowed for stable wires. When the EM strength is higher than the maximum value, the strain energy reduction plus the electrostatic energy reduction due to the patterned electric plate is larger than the volume contribution of the interaction energy. As a consequence, the formation of large wires becomes energetically favorable, and the wires are unstable against size increment [see line 3 of Fig. 8(e)].

The maximum EM strength $\mathcal{J}_{\max}$, as expressed in Eq. (55), increases with decreasing $\hat{H}_f$ and is independent of the stability number $\hat{\Sigma}$. It is further demonstrated in the Appendix that $\mathcal{J}_{\max}$ is always larger than the minimum EM strength $\mathcal{J}_{\min}$ in the viable regime of stable wires. The inequality shows that the two critical values define a range of EM strength for growing stable wires in the viable regime.

C. Size stability of wires

The results in Secs. VI A and VI B reveal that the size stability of wires in the asymptotic cases is determined by two criteria. The first one is the viability criterion expressed in Eq. (48). This criterion evaluates whether or not the SK system can be activated by the electric field to develop stable wires during the EMSO process. Failing the viability criterion indicates stable wires cannot be produced in the SK system during the EMSO process. Satisfying the viability criterion, on the other hand, means stable wires can be generated if the EM strength $\mathcal{J}$ meets the second criterion that $\mathcal{J}$ is in the range of $\mathcal{J}_{\min}$ to $\mathcal{J}_{\max}$,

$$\mathcal{J}_{\min}(\hat{H}_f, \hat{\Sigma}) < \mathcal{J}(\hat{w}_{e0}, \hat{d}, \hat{\mathcal{S}}_e) < \mathcal{J}_{\max}(\hat{H}_f). \tag{56}$$

The lower limit $\mathcal{J}_{\min}$ in Eq. (56) signifies the moment when the patterned electric plate can induce sufficient electrostatic energy reduction so that the formation of wires with a moderate size becomes energetically favorable. In comparison, the upper limit $\mathcal{J}_{\max}$ represents the onset of unstable island growth, which occurs when the reduction of the electrostatic and strain energy exceeds the volume contribution of the interaction energy.

Since $\mathcal{J} \geq 1 + \hat{w}_{e0}/2$, the second criterion imposes an upper bound for the normalized electrostatic energy density $\hat{w}_{e0}$,

$$\hat{w}_{e0} \leq \hat{w}_{e(\max)} = 2\left(\frac{1}{\hat{H}_f^2} - 1\right). \tag{57}$$

As an application, Eqs. (48) and (56) are employed to investigate the size stability of two special cases. In the first case, $\hat{w}_{e0}$, $\hat{d}$, and $\hat{\mathcal{S}}_e$ are given, and the focus is on the domain

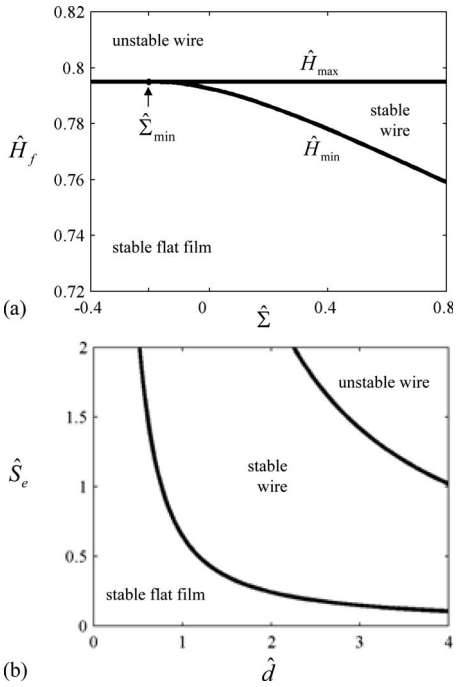

FIG. 11. (a) The stability domain of $(\hat{\Sigma},\hat{H}_f)$ for the case where $\hat{w}_{e0}=0.5$, $\hat{S}_e=1$, and $\hat{d}=1$; (b) the stability domain of $(\hat{d},\hat{S}_e)$ for the case where $\hat{H}_f=0.55$, $\hat{\Sigma}=10$, and $\hat{w}_{e0}=0.5$.

of $(\hat{\Sigma},\hat{H}_f)$ that leads to stable wires. The second case, on the other hand, examines the stability domain of $(\hat{d},\hat{S}_e)$ under the condition that $\hat{w}_{e0}$, $\hat{\Sigma}$, and $\hat{H}_f$ are fixed.

1. Stability domain of $(\hat{\Sigma},\hat{H}_f)$

We examine the first case in this section where $\hat{w}_{e0}$, $\hat{d}$, and $\hat{S}_e$ are given. The three parameters determine the EM strength $\mathcal{J}$ of the system. Substituting $\mathcal{J}$ into the first inequality expressed in Eq. (56) leads to the condition that the film thickness $\hat{H}_f$ has to exceed a minimum value $\hat{H}_{min}$, where

$$\mathcal{J}_{min}(\hat{H}_{min},\hat{\Sigma})=\mathcal{J}. \tag{58}$$

Equation (58) indicates $\hat{H}_{min}$ is a function of $\hat{\Sigma}$ and $\mathcal{J}$.

Similarly, substituting $\mathcal{J}$ into the second inequality in Eq. (56) and evoking Eq. (55) yield $\hat{H}_f<\hat{H}_{max}$, where $\hat{H}_{max}=1/\sqrt{\mathcal{J}}$ is the maximum film thickness allowed for stable wires. In contrast to $\hat{H}_{min}$, $\hat{H}_{max}$ is independent of $\hat{\Sigma}$.

The lower and upper limits of the film thickness are plotted in Fig. 11(a) as functions of $\hat{\Sigma}$ for the case where $\hat{w}_{e0}=0.5$, $\hat{S}_e=1$, and $\hat{d}=1$. (The values of these parameters yield $\mathcal{J}=1.582$.) The results indicate $\hat{H}_{min}$ approaches $\hat{H}_{max}$ as $\hat{\Sigma}$ decreases, and the two limits coincide at $\hat{\Sigma}=\hat{\Sigma}_{min}$, where $\hat{\Sigma}_{min}=-1+1/\sqrt{\mathcal{J}}$. When $\hat{\Sigma}$ is below $\hat{\Sigma}_{min}$, the size stability criterion cannot be satisfied for any film thickness.

The stability diagram of $(\hat{\Sigma},\hat{H}_f)$ for different values of $\mathcal{J}$ would exhibit the same characteristics shown in Fig. 11(a): a stable-wire domain bounded by $\hat{H}_f=\hat{H}_{max}$ and $\hat{H}_f=\hat{H}_{min}$ and the interception of the two boundaries at $\hat{\Sigma}=\hat{\Sigma}_{min}$. These characteristics are also observed in the stability diagram of SK systems without an electric field; see Fig. 7(b).

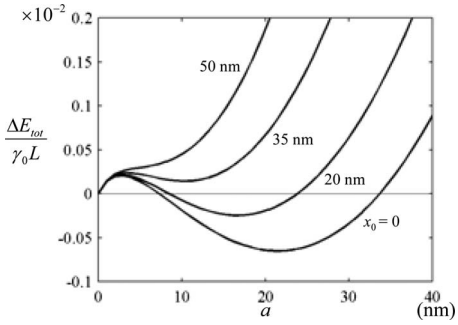

FIG. 12. The effects of pattern-wire misalignment x_0 on the variation of ΔE_{tot} with the wire size a; the parameters of the system are taken to be the same as those for line 3 in Fig. 8(d).

2. Stability domain of $(\hat{d},\hat{S}_e)$

This section investigates the effects of the pattern geometry on the size stability of a viable SK system with a fixed value of $\hat{w}_{e0}$. In this situation, the two parameters of the SK system, namely, $\hat{H}_f$ and $\hat{\Sigma}$, are known, which in turn determine the minimum and the maximum EM strength of the system. Substituting the results and $\hat{w}_{e0}$ into Eq. (56) yields a formula for identifying the domain of $(\hat{d},\hat{S}_e)$ that generates stable wires.

An example of the stability domain is depicted in Fig. 11(b) for the case where $\hat{H}_f=0.55$, $\hat{\Sigma}=10$, and $\hat{w}_{e0}=0.5$. The result indicates the stability domain is bounded by two lines representing the basic and the utmost stable states of the system. It is found that $\hat{d}$ in the stability domain increases with decreasing $\hat{S}_e$.

The stability domain of $(\hat{d},\hat{S}_e)$ is reduced to a range of normalized pattern size $[\hat{d}_{min},\hat{d}_{max}]$ when $\hat{S}_e$ is fixed. The two critical values define the lower and upper limits of the ratio d/H_v for size stability, i.e., $\hat{d}_{min}<d/H_v<\hat{d}_{max}$. The result explains the finding in Fig. 8(b) that the stability diagram of (H_v,d) is bounded by two straight lines in the asymptotic cases.

VII. EFFECTS OF PATTERN-WIRE MISALIGNMENT

The focus of this section turns to the effects of pattern-wire misalignment on the formation of wires. The effects are determined by analyzing the variation of ΔE_{tot} with the wire size a for four values of misalignment, namely, $x_0=0$, 20, 35, and 50 nm. The other parameters of the system are identical to those for line 3 in Fig. 8(d), an example of pattern-induced stable wire.

The results of $\Delta E_{tot}(a)$ for the four values of x_0 are depicted in Fig. 12. The figure indicates ΔE_{tot} exhibits a negative minimum when $x_0=0$ and 20 nm, suggesting the wires at locations with no or small misalignments are stable against

size variation. Comparing the two results of stable wires shows that the depth of the minimum of ΔE_{tot} and thus the size stability of the wire decline with increasing misalignment.

As the misalignment is further increased, the minimum in ΔE_{tot} becomes shallower and its value changes into a positive one; see the result of $x_0=35$ nm. The minimum eventually disappears at sufficiently large misalignments, as indicated in the result of $x_0=50$ nm. A positive minimum or the absence of a minimum means the formation of wires is suppressed energetically.

The results in Fig. 12 provide a clue to the outcomes of preexisting nanostructures when a patterned electric plate is employed to grow stable nanoislands. The outcomes depend on the locations of the preexisting nanostructures. If the locations are in the areas with little influence from the patterns, the preexisting nanostructures possess higher energy than a flat film; as a consequence, the structures would shrink and evolve into a flat film. If the location is in the vicinity of the site aligning with the pattern, on the other hand, the preexisting structure would undergo a self-aligning-organizing process to transform into the aligned stable nanoisland dictated by the pattern.

VIII. DISCUSSION

A. Modification of SK systems for stable nanostructures

In this section we briefly discuss how to modify the SK systems in order to satisfy the viability criterion for stable nanostructures. The approach depends on whether the film is a conductor or a semiconductor. For conductor films, the interaction energy strength B is high; thus, the critical thickness H_1 for the SK transition is large, and $\hat{\Sigma}$ is a positive value. In those systems, the viability criterion can be fulfilled by simply decreasing the film thickness H_f below H_1.

As an example, consider the case where the film is silver, $\epsilon_m=0.02$, $E=83$ GPa, $\nu=0.37$, $\gamma_0=1$ J/m^3, $L=27.7$ nm, $\hat{\gamma}=0.99$, and $\phi=10°$. The interaction energy strength B of silver films was estimated to be 6.62×10^{-10} J/m.[74] Substituting the value of B and the material properties into Eqs. (31) and (30) yields $\hat{\Sigma}=15.4$ and $H_1=7.7$ nm. Since $\hat{\Sigma}>0$, the film would satisfy the viability criterion if H_f is less than $H_1=7.7$ nm.

The large value of H_1 implies $a_{\min}$ can be small even at moderate film thickness. For instance, a film of 4.8 nm ($\hat{H}_f=0.622$) in our current case yields $a_{\min}=12.2$ nm when the electric field is taken to be 0.073 V/nm and the pattern is described by $\hat{d}=2.5$ and $\phi_e=10°$. The size $a_{\min}$ is reduced to 1.86 nm if H_f is equal to 1.5 nm, and a high electric field of 1.29 V/nm is applied.

Turn to the semiconductor film-substrate systems. It is more difficult to meet the viability criterion in those systems because the interaction strength B is much smaller. One possible solution is to enhance the strength by doping the film heavily. It was suggested that the strength B of a SiGe film could reach 5.7×10^{-12} J/m when introducing one atomic percent of donors in the film.[10] This interaction strength can produce $a_{\min}=26$ nm for the case where $L=100$ nm, $\phi=11.3°$, $\hat{\gamma}=0.99$, and $H_f=0.4$ nm, which roughly corresponds to the SiGe film with 25% of Ge in atomic concentration. The equilibrium island size can be further reduced if the interaction strength can be increased significantly. This, however, requires a different interaction mechanism, a crucial issue that needs to be explored in the future.

B. Kinetics

After discussing the possible approaches for satisfying the size stability criteria, we comment briefly in this section whether or not the stable nanostructures can develop during a typical annealing process where surface diffusion is the dominating kinetic mechanism. To answer this question, it is helpful to compare the simulation results in Refs. 66 and 87. Both adopted the same model for the SK systems to study the growth of nanoislands driven by the surface diffusion mechanism, while the two works differed in the electric field: Reference 66 took into account the effects of the electric field generated by a patterned electric plate; in contrast, Ref. 87 focused on the cases where the electric field is absent. The comparison of the two works reveals that the growth of nanoislands under a patterned electric plate is much faster than that without the electric field.[88] Since the latter can be observed in experiments routinely, the patterned-induced island formation is expected to be feasible.

The effect of a pattern on the growth rate of nanostructures can be understood as follows. The growth of nanostructures in SK systems without an electric field is driven by the strain energy reduction, and it follows from Eq. (3) that the corresponding energetic force for island growth is given by the negative of the strain energy density $-w(x)$. (This is analogous to the energetic force due to the electrostatic energy discussed in Sec. II D.) This energetic force, as expressed in Eq. (1), increases with the slope and size of the nanostructure. Thus, the energetic force for island growth is small when the film morphology is a slightly rough surface profile.

The pattern on the electric plate, on the contrary, induces an energetic force that is independent of the geometry of the nanoislands on the film surface (see Sec. II D). This energetic force can be large even when the nanostructures on the film are still shallow and/or small. This explains why the pattern can accelerate the growth of nanostructures drastically.

C. Controlled growth of nanoislands

The size stability analyses presented in this paper illustrate a potential method for controlling the self-assembly of nanostructures. The first step is to choose a system that can satisfy the viability criterion given in Eq. (48). The system can be a coarsening one characterized by $\hat{\Sigma}<0$ or a stable one with $\hat{\Sigma}>0$, while the stable one is a better choice since it allows a larger thickness range for fabricating stable nanostructures.

The stable SK system can develop stable wires without an

electric field if the normalized thickness $\hat{H}_f$ is in the range $\hat{H}_E < \hat{H}_f < 1$, where $\hat{H}_E$ is defined earlier in Fig. 7. This range, however, is unsuitable for controlling the island growth since the nanostructures can develop at any location on the film surface.

The controllable self-assembly of nanoislands is achieved by using films in the thickness range $\hat{H}_f < \hat{H}_E$ together with a patterned electric plate. In this design, the flat film is the equilibrium morphology in the areas with little influence from the patterns, while the flat film is transformed into stable nanostructures in the area affected by the pattern. The transformation can occur if the EM strength $\mathcal{J}$ due to the patterns satisfies the criterion expressed in Eq. (56), which in turn defines a stability domain of the pattern parameters [see for example the stability domain of $(\hat{d}, \hat{\mathcal{S}}_e)$ of nanowires discussed in Sec. VI C]. Varying the pattern geometry within the stability domain leads to different sizes and shapes of stable nanostructures at the specified locations.

For a given SK system, $\hat{\Sigma}$ is fixed, and the smallest size of stable nanostructures $\hat{a}_{\min}$ can be reduced by decreasing the normalized thickness $\hat{H}_f$; see Fig. 9(b). Decreasing $\hat{H}_f$, however, causes $\mathcal{J}_{\min}$ and thus the electric field to increase; see Fig. 9(a). The electric field can become too high to be feasible in the actual systems, and this imposes a constraint on the smallest film thickness that can be attained in the process.

D. Limitations

The analyses presented in this paper provide a simple scheme for determining the size stability of wires under the influence of a patterned electric plate. The scheme, nevertheless, overlooks several issues that can affect the size stability. For example, the formulas adopted here for calculating the strain and electrostatic energy changes are accurate to the first order of the wire slope. This is valid for shallow islands, while the effects of large wire slopes have to be included in order to have more accurate predictions of the size stability.

Besides the large slopes, other issues that need to be considered include the kinetics of the EMSO process, the surface stress, other mechanisms of the interaction energy, and the electrostatics of semiconductor films. Understanding these issues is essential for developing technologies that can control the growth of nanoislands in the SK systems.

IX. SUMMARY

This paper investigates the stability of wires against size variation during the EMSO process. The investigation starts with the case where the electric field is absent from the process. In such a case, the wire is stable against size variation if the normalized stability number $\hat{\Sigma}$ is positive and the normalized film thickness $\hat{H}_f$ is within the range $[\hat{H}_E, 1]$. The variation of the thickness range with $\hat{\Sigma}$ is illustrated in Fig. 7(b).

The investigation then turns to a typical example of a coarsening SK system to study the effects of d and H_v on the size stability of wires that align with the pattern. The results show that the coarsening system can be activated to develop stable wires of different sizes when the pattern size d and the electric plate height H_v are in the stable-wire regime depicted in Fig. 8(b). The results also indicate the upper limit of the wire size $a_{\mathrm{eq(max)}}$ increases with H_v, while the lower limit $a_{\mathrm{eq(min)}}$ is insensitive to the parameters of the electric field.

Motivated by the findings in the specific example, the investigation further explores the wire size stability of the asymptotic cases where the pattern size d and the electric plate height H_v are large. The size stability is shown to be determined by two criteria. The first one, the viability criterion given in Eq. (48), evaluates whether or not the SK system can be activated by the electric field to generate stable wires.

The second criterion, expressed in Eq. (56), requires that the EM strength $\mathcal{J}$ is in the range $[\mathcal{J}_{\min}, \mathcal{J}_{\max}]$. The minimum EM strength $\mathcal{J}_{\min}$ corresponds to the moment when the patterned electric plate can induce sufficient electrostatic energy reduction so that the wire formation becomes energetically favorable for moderate size. The minimum EM strength $\mathcal{J}_{\min}$ depends on the normalized film thickness $\hat{H}_f$ and the normalized stability number $\hat{\Sigma}$; the variation of $\mathcal{J}_{\min}$ with the two parameters is depicted in Fig. 9(a). In comparison, the maximum EM strength $\mathcal{J}_{\max}$ signifies that the reduction of the electrostatic and strain energy exceeds the volume contribution of the interaction energy, leading to unstable growth of large wires. The maximum EM strength is expressed in Eq. (55), indicating $\mathcal{J}_{\max}$ increases with decreasing $\hat{H}_f$.

In addition to the cases of aligned wires, the effects of the pattern-wire misalignment on the formation and the stability of wires are also examined. It is found that the wire at the site aligning with the pattern has the lowest energy and the highest size stability. As the misalignment increases, the energy increases and the stability declines. At sites with large misalignment, the formation of wire is completely suppressed. The results demonstrate the potential of using patterns to fabricate nanostructures stable against size variation at specified locations.

ACKNOWLEDGMENTS

The project was supported by National University of Singapore (Grant No. R-284-000-006-112). The authors are grateful to X.-S. Wang and D. Chua for helpful discussions.

APPENDIX: THE BASIC STABLE STATES IN THE VICINITY OF $\hat{H}_f = 1 + \hat{\Sigma}$

The Appendix first derives $\hat{a}_{\min}$ and $\mathcal{J}_{\min}$ of the basic stable states in the vicinity of the boundary $\hat{H}_f = 1 + \hat{\Sigma}$. The result of $\mathcal{J}_{\min}$ is then compared with $\mathcal{J}_{\max}$ to demonstrate that $\mathcal{J}_{\max} > \mathcal{J}_{\min}$ except on the boundary where the two limits coincide.

When studying the basic stable states in the vicinity of the boundary $\hat{H}_f = 1 + \hat{\Sigma}$, it is convenient to express the coefficient $\hat{c}_1$ as $\hat{c}_1 = -\epsilon$ where ϵ is a positive number with small magnitude. Substituting the expression into Eq. (45) and employing the change of variable $t = \hat{a}_{\min}\epsilon$ reduce $\Delta\hat{E}_{\mathrm{tot}}$ given in Eq. (45) to

$$\Delta\hat{E}_{\text{tot}} = \ln t - \ln \epsilon - t + \frac{\hat{c}_2 t^2}{\epsilon^2}. \tag{A1}$$

The minimum point of $\Delta\hat{E}_{\text{tot}}$ is determined by solving the equation $\Delta\hat{E}_{\text{tot}}(t)=0$, which can be rewritten as

$$\frac{\hat{c}_2 t^2}{\epsilon^2} - \frac{t}{2} + \frac{1}{2} = 0. \tag{A2}$$

According to Eq. (A2), $\Delta\hat{E}_{\text{tot}}$ at the minimum point can be calculated to be

$$\Delta\hat{E}_{\text{min}} = \ln t - \ln \epsilon - \frac{t}{2} - \frac{1}{2}. \tag{A3}$$

It can be verified later that $t \gg 1$ at small values of ϵ. Thus, $t \gg \ln t$, $|\ln \epsilon| \gg 1/2$, and $\Delta\hat{E}_{\text{min}}$ can be further simplified to

$$\Delta\hat{E}_{\text{min}} = -\ln \epsilon - \frac{t}{2}. \tag{A4}$$

The minimum $\Delta\hat{E}_{\text{min}}$ vanishes at the basic stable states, leading to the solution $t=-2\ln\epsilon$. The result confirms the assertion that $t \gg 1$ as $\epsilon \to 0$. The result also determines the stable-wire size $\hat{a}_{\text{min}}$ in the vicinity of the boundary to be

$$\hat{a}_{\text{min}} = \frac{-2\ln\epsilon}{\epsilon}. \tag{A5}$$

Equation (A5) explains the result depicted in Fig. 9(b) that $\hat{a}_{\text{min}}$ increases drastically when approaching the boundary $\hat{H}_f = 1 + \hat{\Sigma}$.

Substituting the solution of t into Eq. (A2) and ignoring the smallest term $-1/2$ yields

$$\hat{c}_2 = \frac{\epsilon^2}{2t} = -\frac{\epsilon^2}{4\ln\epsilon}. \tag{A6}$$

Comparing Eq. (A6) with Eq. (35) gives the required minimum EM strength $\mathcal{J}_{\text{min}}$ in the vicinity of the boundary $\hat{H}_f = 1 + \hat{\Sigma}$,

$$\mathcal{J}_{\text{min}} = \left(1 + \frac{\epsilon^2}{2\ln\epsilon}\right)\frac{1}{\hat{H}_f^2}. \tag{A7}$$

On the boundary, $\epsilon=0$ and $\mathcal{J}_{\text{min}}|_{\epsilon=0} = 1/\hat{H}_f^2 = \mathcal{J}_{\text{max}}$. In other words, the asymptotic lower and upper limits of the EM strength coincide on the boundary $\hat{H}_f = 1 + \hat{\Sigma}$.

Except on the boundary $\hat{H}_f = 1 + \hat{\Sigma}$, the lower and upper limits are different. In particular, $\mathcal{J}_{\text{min}}$ decreases if $\hat{H}_f$ is fixed but $\hat{\Sigma}$ increases [see Fig. 9(a) and Eq. (A7)]. On the other hand, $\mathcal{J}_{\text{max}}$ remains the same as long as $\hat{H}_f$ is fixed. This demonstrates that $\mathcal{J}_{\text{max}} \geq \mathcal{J}_{\text{min}}$ in the viable regime for the stable wires.

*msecch@nus.edu.sg

[1] D. J. Eaglesham and M. Cerullo, Phys. Rev. Lett. **64**, 1943 (1990).
[2] Y.-W. Mo, D. E. Savage, B. S. Swartzentruber, and M. G. Lagally, Phys. Rev. Lett. **65**, 1020 (1990).
[3] F. M. Ross, J. Tersoff, and R. M. Tromp, Phys. Rev. Lett. **80**, 984 (1998).
[4] F. M. Ross, R. M. Tromp, and M. C. Reuter, Science **286**, 1931 (1999).
[5] J. A. Floro, M. B. Sinclair, E. Chason, L. B. Freund, R. D. Twesten, R. Q. Hwang, and G. A. Lucadamo, Phys. Rev. Lett. **84**, 701 (2000).
[6] V. A. Shchukin, N. N. Ledentsov, P. S. Kop'ev, and D. Bimberg, Phys. Rev. Lett. **75**, 2968 (1995).
[7] I. Daruka and A.-L. Barabasi, Phys. Rev. Lett. **79**, 3708 (1997).
[8] G. Medeiros-Ribeiro, A. M. Bratkovski, T. I. Kamins, D. A. A. Ohlberg, and R. S. Williams, Science **279**, 353 (1998).
[9] C.-h. Chiu, Appl. Phys. Lett. **75**, 3473 (1999).
[10] C.-h. Chiu, Phys. Rev. B **69**, 165413 (2004).
[11] Q. Xie, A. Madhukar, P. Chen, and N. P. Kobayashi, Phys. Rev. Lett. **75**, 2542 (1995).
[12] J. Tersoff, C. Teichert, and M. G. Lagally, Phys. Rev. Lett. **76**, 1675 (1996).
[13] N. N. Ledentsov *et al.*, Phys. Rev. B **54**, 8743 (1996).
[14] G. Springholz, V. Holy, M. Pinczolits, and G. Bauer, Science **282**, 734 (1998).
[15] R. Heitz, A. Kalburge, Q. Xie, M. Grundmann, P. Chen, A. Hoffmann, A. Madhukar, and D. Bimberg, Phys. Rev. B **57**, 9050 (1998).
[16] V. Le Thanh, V. Yam, P. Boucaud, F. Fortuna, C. Ulysse, D. Bouchier, L. Vervoort, and J. M. Lourtioz, Phys. Rev. B **60**, 5851 (1999).
[17] O. G. Schmidt and K. Eberl, Phys. Rev. B **61**, 13721 (2000).
[18] H. Lee, J. A. Johnson, M. Y. He, J. S. Speck, and P. M. Petroff, Appl. Phys. Lett. **78**, 105 (2001).
[19] G. Capellini, M. De Seta, C. Spinella, and F. Evangelisti, Appl. Phys. Lett. **82**, 1772 (2003).
[20] M. Schmidbauer, S. Seydmohamadi, D. Grigoriev, Z. M. Wang, Y. I. Mazur, P. Schafer, M. Hanke, R. Kohler, and G. J. Salamo, Phys. Rev. Lett. **96**, 066108 (2006).
[21] C.-h. Chiu and H. Wang, Phys. Rev. B **75**, 125416 (2007).
[22] S. Y. Shiryaev, F. Jensen, J. L. Hansen, J. W. Petersen, and A. N. Larsen, Phys. Rev. Lett. **78**, 503 (1997).
[23] Y. H. Xie, S. B. Samavedam, M. Bulsara, T. A. Langdo, and E. A. Fitzgerald, Appl. Phys. Lett. **71**, 3567 (1997).
[24] A. E. Romanov, P. M. Petroff, and J. S. Speck, Appl. Phys. Lett. **74**, 2280 (1999).
[25] F. Leroy, J. Eymery, and P. Gentile, Appl. Phys. Lett. **80**, 3078 (2002).
[26] V. Poydenot, R. Dujardin, J. L. Rouvière, A. Barski, J. Mezière, and F. Fournel, Surf. Sci. **600**, L135 (2006).
[27] A. Pascale, P. Gentile, J. Eymery, J. Mezière, A. Bavard, T. U. Schülli, and F. Fournel, Surf. Sci. **600**, 3187 (2006).
[28] T. I. Kamins and R. S. Williams, Appl. Phys. Lett. **71**, 1201

(1997).
[29] T. I. Kamins, D. A. A. Ohlberg, R. S. Williams, W. Zhang, and S. Y. Chou, Appl. Phys. Lett. **74**, 1773 (1999).
[30] R. Zhang, R. Tsui, K. Shiralagi, D. Convey, and H. Goronkin, Appl. Phys. Lett. **73**, 505 (1998).
[31] A. Konkar, A. Madhukar, and P. Chen, Appl. Phys. Lett. **72**, 220 (1998).
[32] G. Jin, J. L. Liu, and K. L. Wang, Appl. Phys. Lett. **76**, 3591 (2000).
[33] H. Lee, J. A. Johnson, J. S. Speck, and P. M. Petroff, J. Vac. Sci. Technol. B **18**, 2193 (2000).
[34] T. Kitajima, B. Liu, and S. R. Leone, Appl. Phys. Lett. **80**, 497 (2002).
[35] B. Yang, F. Liu, and M. G. Lagally, Phys. Rev. Lett. **92**, 025502 (2004).
[36] O. G. Schmidt, N. Y. Jin-Phillipp, C. Lange, U. Denker, K. Eberl, R. Schreiner, H. Grabeldinger, and H. Schweizer, Appl. Phys. Lett. **77**, 4139 (2000).
[37] Z. Zhong, A. Halilovic, T. Fromherz, F. Schäffler, and G. Bauer, Appl. Phys. Lett. **82**, 4779 (2003).
[38] S. Kiravittaya, H. Heidemeyer, and O. G. Schmidt, Physica E (Amsterdam) **23**, 253 (2004).
[39] G. Chen, H. Lichtenberger, G. Bauer, W. Jantsch, and F. Schäffler, Phys. Rev. B **74**, 035302 (2006).
[40] N. D. Machtay and R. V. Kukta, J. Appl. Mech. **73**, 212 (2006).
[41] Y. Nitta, M. Shibata, K. Fujita, and M. Ichikawa, Surf. Sci. **462**, L587 (2000).
[42] J. J. Eggleston and P. W. Voorhees, Appl. Phys. Lett. **80**, 306 (2002).
[43] T.-S. Yoon, Z. Zhao, J. Liu, Y.-H. Xie, D. y. Ryu, T. P. Russell, H.-M. Kim, and K.-B. Kim, Appl. Phys. Lett. **89**, 063107 (2006).
[44] M. Kammler, R. Hull, M. C. Reuter, and F. M. Ross, Appl. Phys. Lett. **82**, 1093 (2003).
[45] C.-h. Chiu, Z. Huang, and C. T. Poh, Phys. Rev. Lett. **93**, 136105 (2004).
[46] Z. G. Xie and G. S. Solomon, Appl. Phys. Lett. **87**, 093106 (2005).
[47] J. T. Robinson, J. A. Liddle, A. Minor, V. Radmilovic, and O. D. Dubon, J. Cryst. Growth **287**, 518 (2006).
[48] J. h. Zhu, K. Brunner, and G. Abstreiter, Appl. Phys. Lett. **73**, 620 (1998).
[49] X. Deng and M. Krishnamurthy, Phys. Rev. Lett. **81**, 1473 (1998).
[50] J. D. Weil, X. Deng, and M. Krishnamurthy, J. Appl. Phys. **83**, 212 (1998).
[51] M. Borgström, V. Zela, and W. Seifert, Nanotechnology **14**, 264 (2003).
[52] R. Songmuang, S. Kiravittaya, and O. S. Schmidt, Appl. Phys. Lett. **82**, 2892 (2003).
[53] J. L. Gray, R. Hull, and J. A. Floro, Appl. Phys. Lett. **81**, 2445 (2002).
[54] J. L. Gray, N. Singh, D. M. Elzey, R. Hull, and J. A. Floro, Phys. Rev. Lett. **92**, 135504 (2004).
[55] J. L. Gray, R. Hull, C.-H. Lam, P. Sutter, J. Means, and J. A. Floro, Phys. Rev. B **72**, 155323 (2005).
[56] S. Y. Chou, L. Zhuang, and L. Guo, Appl. Phys. Lett. **75**, 1004 (1999).
[57] E. Schäffer, T. Thurn-Albrecht, T. P. Russell, and U. Steiner, Nature (London) **403**, 874 (2000).
[58] Z. Lin, T. Kerle, S. M. Baker, D. A. Hoagland, E. Schäffer, U. Steiner, and T. P. Russell, J. Chem. Phys. **114**, 2377 (2001).
[59] P. Deshpande and S. Y. Chou, J. Vac. Sci. Technol. B **19**, 2741 (2001).
[60] M. Morariu, N. Voicu, E. Schäffer, Z. Lin, T. P. Russell, and U. Steiner, Nat. Mater. **2**, 48 (2003).
[61] R. Verma, A. Sharma, K. Kargupta, and J. Bhaumik, Langmuir **21**, 3710 (2005).
[62] D. Kim and W. Lu, Phys. Rev. B **73**, 035206 (2006).
[63] L. F. Pease III and W. B. Russel, Langmuir **20**, 795 (2004).
[64] J. Liang and Z. Suo, Appl. Phys. Lett. **79**, 3251 (2001).
[65] K. A. Leach, Z. Lin, and T. P. Russell, Macromolecules **38**, 4868 (2005).
[66] C.-h. Chiu, Z. Huang, and C. T. Poh, Phys. Rev. B **73**, 193409 (2006).
[67] C.-h. Chiu and C. T. Poh, Phys. Rev. B **71**, 045406 (2005).
[68] H. Gao, Int. J. Solids Struct. **28**, 703 (1991).
[69] I. Daruka, J. Tersoff, and A.-L. Barabási, Phys. Rev. Lett. **82**, 2753 (1999).
[70] J. Tersoff and R. M. Tromp, Phys. Rev. Lett. **70**, 2782 (1993).
[71] J. D. Eshelby, in *Inelastic Behavior of Solids*, edited by M. F. Kanninen (McGraw-Hill, New York, 1970), p. 78.
[72] J. R. Rice, J. Appl. Mech. **35**, 379 (1968).
[73] J. Tersoff, Phys. Rev. B **43**, 9377 (1991).
[74] Z. Suo and Z. Zhang, Phys. Rev. B **58**, 5116 (1998).
[75] If the thickness is below the minimum value, the volume contribution of the interaction energy is so large that the wire formation of any size is completely suppressed.
[76] Equation (15) is similar to the result of the strain energy change due to the nanostructure formation on the film surface under the influence of a preexisting embedded island; see Eq. (15) in Ref. 21. A coefficient 2 is also found in the term that represents the effect of the preexisting embedded island.
[77] C.-h. Chiu and Z. Huang, J. Appl. Phys. **103**, 063503 (2008).
[78] E. Schäffer, T. Thurn-Albrecht, T. P. Russell, and U. Steiner, Europhys. Lett. **53**, 518 (2001).
[79] L. F. Pease III and W. B. Russel, J. Chem. Phys. **118**, 3790 (2003).
[80] D. Du and D. Srolovitz, Appl. Phys. Lett. **85**, 4917 (2004).
[81] F. Yang and W. Song, Appl. Phys. Lett. **87**, 111912 (2005).
[82] N. Y. Chien, H. Gao, G. Herrmann, and D. M. Barnett, Proc. R. Soc. London, Ser. A **452**, 527 (1996).
[83] For systems characterized by coarsening wires, the patterns result in more reduction of electrostatic energy and accordingly a higher rate of the coarsening process.
[84] More specifically, $\Delta\hat{E}_{\text{tot}}$ in the area between $\hat{H}_f=\hat{H}_E$ and $\hat{H}_f=\hat{H}_Q$ is represented by line 1B, and $\Delta\hat{E}_{\text{tot}}$ below $\hat{H}_f=\hat{H}_Q$ is characterized by line 1A.
[85] That the solution $\mathcal{J}_{\min}$ is the minimum EM strength for stable wires can be understood as follows. For given $\hat{H}_f$ and $\hat{\Sigma}$, the total energy change $\Delta\hat{E}_{\text{tot}}$ is a function of $\hat{a}$ and $\mathcal{J}$. Thus, the variation of $\Delta\hat{E}_{\text{tot}}$ with $\hat{a}$ and $\mathcal{J}$ in the vicinity of the basic stable states can be expressed as $\Delta\hat{E}_{\text{tot}}=\Delta\hat{E}_{\text{tot}}(\hat{a}_{\min},\mathcal{J}_{\min})+(\partial\Delta\hat{E}_{\text{tot}}/\partial\hat{a})\Delta\hat{a}+(\partial\Delta\hat{E}_{\text{tot}}/\partial\mathcal{J})\Delta\mathcal{J}$. The first two terms in the expression are zero in the basic stable states, leading to $\Delta\hat{E}_{\text{tot}}=-(\mathcal{J}_{\min}\hat{H}_f^2\hat{a}_{\min}^2/2)\Delta\mathcal{J}$. Requiring the total energy change $\Delta\hat{E}_{\text{tot}}$ to be negative yields $\Delta\mathcal{J}=\mathcal{J}-\mathcal{J}_{\min}>0$, confirming $\mathcal{J}_{\min}$ is the minimum EM strength for stable wires.
[86] For the SK systems in this area of $(\hat{\Sigma},\hat{H}_f)$, the film can develop into two types of film morphology, namely, the stable wire and

the unstable wire, while the stable flat film cannot occur for any combination of H_v, d, and w_{e0}.

[87] C.-h. Chiu and Z. Huang, J. Appl. Phys. **101**, 113540 (2007).

[88] References 66 and 87 present the results in terms of the normalized time t/t_L, where t_L is defined by the same formula in both papers. It is found that the normalized time t/t_L for the formation of nanostructures during the EMSO process is less than 5×10^{-4}; see Fig. 3 of Ref. 66. The results plotted in Fig. 1 of Ref. 87, on the other hand, suggest the normalized formation time t/t_L is about 0.5 during the annealing process without an electric field.